Hindawi
Advances in Civil Engineering
Volume 2020, Article ID 8850688, 24 pages
https://doi.org/10.1155/2020/8850688

Research Article

Study of Wind Loads and Wind Speed Amplifications on High-Rise Building with Opening by Numerical Simulation and Wind Tunnel Test

Fu-Bin Chen,[1,2] Xiao-Lu Wang,[1,2] Yun Zhao,[1,2] Yuan-Bo Li,[1,2] Qiu-Sheng Li,[3,4] Ping Xiang,[4] and Yi Li[5]

[1]*National-Local Joint Engineering Laboratory of Technology for Long-Term Performance Enhancement of Bridges in Southern District, Changsha University of Science and Technology, Changsha, Hunan 410114, China*
[2]*Hunan Provincial Key Laboratory of Green Construction and Maintenance of Bridge and Building, Changsha University of Science and Technology, Changsha, Hunan 410114, China*
[3]*Department of Architecture and Civil Engineering, City University of Hong Kong, Kowloon, Hong Kong*
[4]*School of Civil Engineering, Central South University, Changsha, Hunan 410075, China*
[5]*Hunan Provincial Key Laboratory of Structures for Wind Resistance and Vibration Control and School of Civil Engineering, Hunan University of Science and Technology, Xiangtan, Hunan 411201, China*

Correspondence should be addressed to Yi Li; liyi1988@hnust.edu.cn

Received 5 June 2020; Accepted 8 September 2020; Published 29 September 2020

Academic Editor: Claudio Mazzotti

High-rise buildings are very sensitive to wind excitations, and wind-induced responses have always been the key factors for structural design. Facade openings have often been used as aerodynamic measures for wind-resistant design of high-rise buildings to meet the requirement of structural safety and comfort. Obvious wind speed amplifications can also be observed inside the openings. Therefore, implementing wind turbines in the openings is of great importance for the utilization of abundant wind energy resources in high-rise buildings and the development of green buildings. Based on numerical simulation and wind tunnel testing, the wind loads and wind speed amplifications on high-rise buildings with openings are investigated in detail. The three-dimensional numerical simulation for wind effects on high-rise building with openings was firstly carried out on FLUENT 15.0 platform by SST k − ε model. The mean wind pressure coefficients and the wind flow characteristics were obtained. The wind speed amplifications at the opening were analyzed, and the distribution law of wind speed in the openings is presented. Meanwhile, a series of wind tunnel tests were conducted to assess the mean and fluctuating wind pressure coefficients in high-rise building models with various opening rates. The variation of wind pressure distribution at typical measuring layers with wind direction was analyzed. Finally, the wind speed amplifications in the openings were studied and verified by the numerical simulation results.

1. Introduction

With the development of science and technology, new materials with light weight and high strength have been emerged. This promotes to the high-rise buildings in the trend of light weight, high flexibility, and low damping. High-rise buildings are sensitive to wind excitations. Wind loads are the key factor for structural design of high-rise buildings [1–4]. For super high-rise buildings, the wind-induced responses caused by across-wind vibration will exceed those caused by along-wind force [5]. How to reduce wind effects on high-rise buildings has always been the hot issue in wind engineering [6–11].

In recent years, openings have been adopted for wind loads reduction of high-rise buildings [12–14]. Li et al. investigated wind load characteristics of high-rise buildings with opening. Bearman believed that the opening directly directed the airflow to the side and back areas of the structure, which could break the regular vortex shedding system closely related to the across-wind response [15]. Kikitsu and Okada showed that openings could reduce the structural dynamic response of high-rise buildings

[16]. Dutton and Isyumov conducted a wind tunnel testing on a tall building with a 9:1 aspect ratio of the square cross section and pointed out that openings can be effective in reducing the across-wind excitation of tall buildings [17]. Okada and Kong carried out aeroelastic tests on square buildings with three opening modes and concluded that opening rate of 1.5% can reduce the dynamic displacement of the across-wind direction by 20%–25% [18]. Zhang et al. indicated that the primary factor for the reduction of overall wind load on building models was the decrease of surface area due to opening [19]. Hu et al. pointed out that openings reduced the wind-induced response significantly in the across-wind direction [20]. With the increasing concerns on energy crisis, openings in the high-rise buildings are getting more attraction for wind power generation. Li et al. pointed out that the openings could result in wind speed amplifications to some extent and would be of benefit for wind turbine installation for the purpose of wind energy utilization [21, 22]. Besides the reduction of aerodynamic forces, researchers began to focus on the flow characteristics around the high-rise building with opening. Hassanli et al. investigated mean flow characteristics and the flow structure inside openings with five different layout configurations for wind energy harvesting [23]. Based on numerical simulation, Wang et al. analyzed the surface pressure contour and wind pressure coefficients of high-rise building with openings [24].

Both numerical simulation and wind tunnel testing are adopted in this study to evaluate the effects of opening on high-rise building. The mean wind pressure coefficients and the wind flow characteristics are discussed. The distribution law of wind speed in the openings is presented. Moreover, the wind speed amplifications at the opening are analyzed and comparatively studied. This study aims to provide useful information for wind-resistant design and wind energy utilization of high-rise building with openings.

2. Numerical Simulation

In order to investigate the wind effect of high-rise building with openings, four rectangular models ($B \times D \times H = 120\,\text{mm} \times 120\,\text{mm} \times 600\,\text{mm}$) were established in the numerical simulation software FLUENT 15.0, which are, respectively, named as L-1 (fully enclosed), L-2 (large openings in x-direction), L-3 (large openings in both x- and y-directions), and S-1 (small openings in both x- and y-directions). The opening heights are set at 0.51 H and 0.85 H, respectively, as shown in Figure 1.

The computational domain was set as $7920\,\text{mm} \times 2040\,\text{mm} \times 1800\,\text{mm}$, as shown in Figure 2. In the height of the 0.51 H and 0.85 H of the L-3 model, a total of 21 monitoring points, which were recorded as a_1–a_{11} and b_1–b_{11}, were used for wind speed monitoring, as shown in Figure 3. Monitoring points a_1–a_{11} are set in the x-direction openings, while monitoring points b_1–b_{11} are set in the y-direction openings. The wind direction was also defined in Figure 3.

2.1. Mean Wind Pressure Coefficients. Figure 4 illustrates the mean wind pressure coefficients of L-1, L-2, and L-3 models under wind direction of 0°, respectively. It can be found that the mean wind pressure coefficients of the windward face are positive, and the fully enclosed model L-1 reaches the maximum value 0.95 in the upper part of the building. After the openings are set, the local mean wind pressure coefficients increase at the top of the upper opening but decrease below the upper opening. The mean wind pressure coefficients are reduced near the lower opening. The other mean wind pressure coefficients away from the openings are almost unchanged.

The mean wind pressure coefficients on the side faces are negative and change little along the elevation. Compared with the L-1 model, the mean wind pressure coefficients on side faces of L-2 model are reduced. As for the L-3 model, the mean wind pressure coefficients decrease further, and the flow fields near the openings change. The wind pressure distribution at the inner openings changes.

The mean wind pressure coefficients on the leeward faces are also negative. For L-1 model, the mean wind pressure coefficients at the bottom are the smallest and increase gently with elevation. After the openings are set, the negative pressures on the leeward tend to decrease as a whole. The mean wind pressure coefficients increase in circumferential direction far from the openings, and the maximum value of negative pressure appears near the openings.

Figures 5 and 6 show the mean wind pressure distribution in the openings of L-2 model and L-3 model, respectively. For L-2 model, large negative pressures are generated at the leading edge of the openings. The absolute value of the negative pressure decreases along the incoming flow direction. The mean wind pressure coefficients in the trailing edge of the upper opening are uniformly maintained at about −0.5 while those of the lower opening are maintained at around −0.45. As for the L-3 model, the absolute value of the negative pressures on the inner wall of the x-direction opening is significantly increased, indicating that the wind speed in the opening is further accelerated.

2.2. Wind Flow Characteristics

2.2.1. Flow Field at the Same Elevation. The flow separation, vortex shedding phenomenon on the side face, and wake flow downstream the leeward can be visible in the numerical simulation. The mean velocity contour distributions with streamlines at height of 0.85 H for L-1 model, L-2 model, and L-3 model under wind direction of 0° are, respectively, presented in Figure 7. For L-1 model, flow separations are obviously found on the side faces, and regular large-scale vortexes are observed downstream the leeward. For L-2 model, the incoming flow is accelerated through the opening and disturbs the regular vortexes downstream leeward. New small-scale vortexes are formed near the opening. Moreover, the wind speeds along the side faces are decreased. When the openings are set at both x-direction and y-direction for L-3 model, except for the complex flow characteristics emerged at y-direction openings, the regular vortexes downstream leeward are also disturbed. The sizes of vortexes on the side faces are decreased compared with L-2 model.

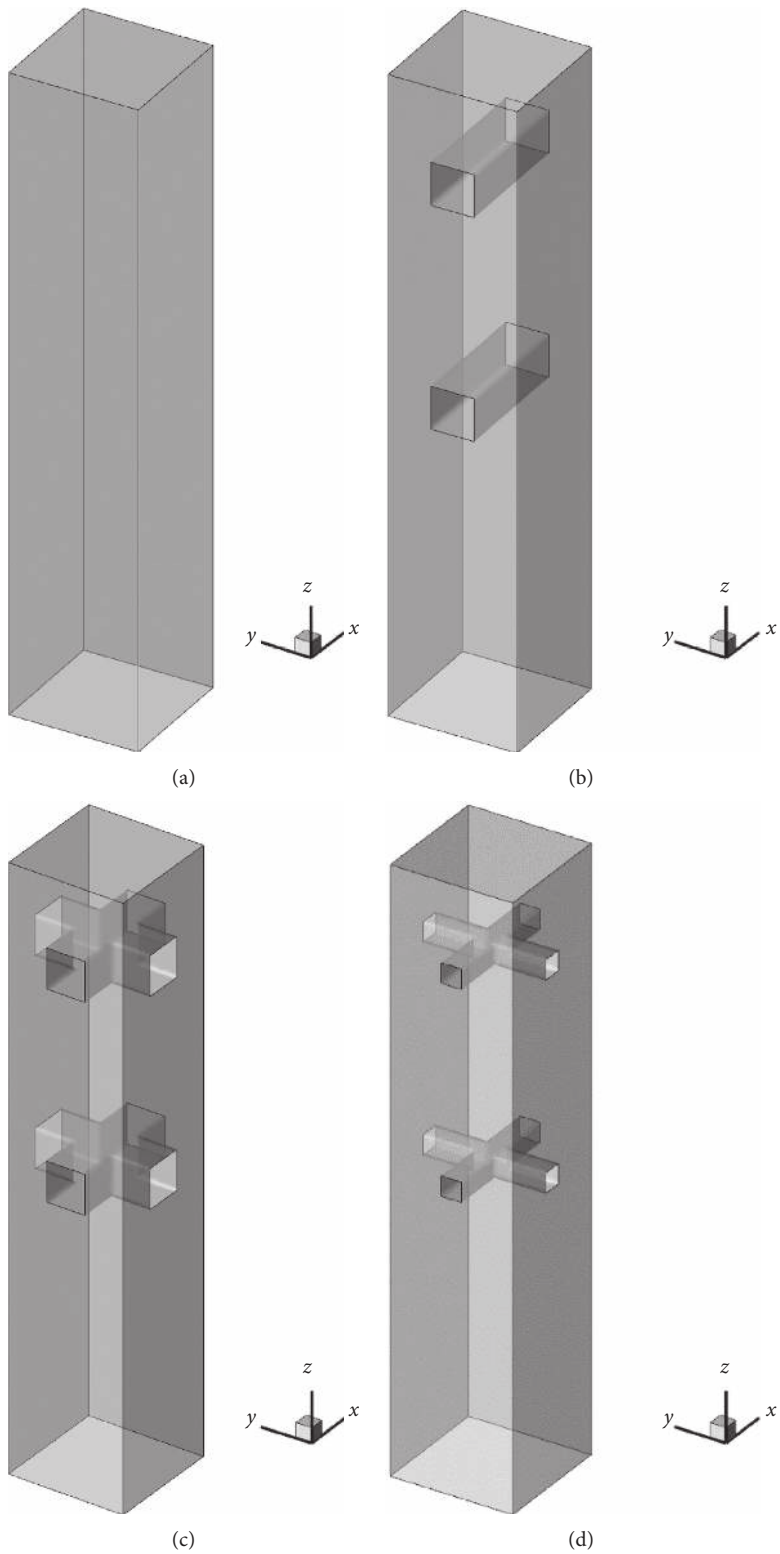

Figure 1: Four kinds of numerical simulation models with openings. (a) L-1. (b) L-2. (c) L-3. (d) S-1.

2.2.2. Flow Field at Different Elevations. Figure 8 shows the mean wind pressure contour distributions on windward and leeward faces at different elevations for L-1 model, L-2 model, and L-3 model under wind direction of 0°, respectively. For L-1 model, the wind flow strikes the windward and creates a stagnation point at about 2/3 height of model. The maximum positive pressure is emerged near the stagnation point. After the openings are set, the flow at the opening position is introduced into the leeward face, and the positive pressure near the opening is decreased. The single

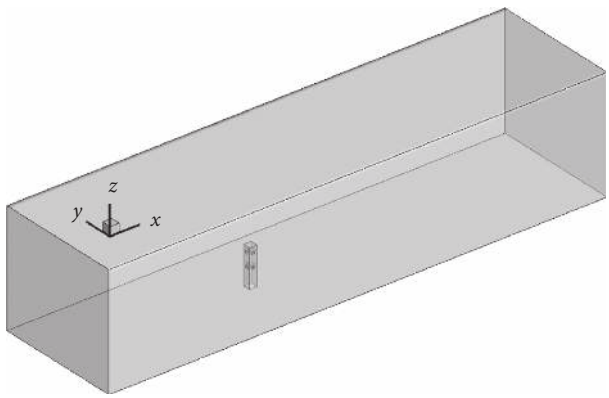

Figure 2: The computational domain in FLUENT.

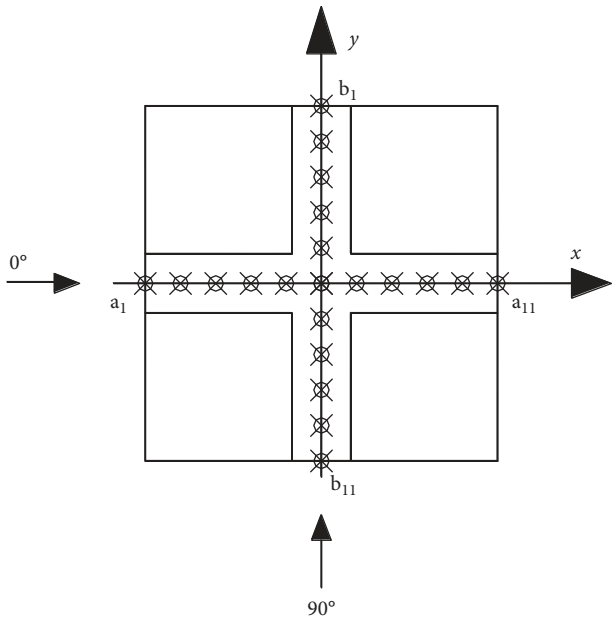

Figure 3: Monitoring points in the opening and wind direction definition.

vortex on the top from the leeward is shattered and reduced to four different vortexes, which results in the phenomenon that the mean wind pressure coefficients on the leeward face decrease in circumferential direction away from the openings. The flow field characteristics of L-3 model are consistent with those of L-2 model on the windward and leeward. However, the absolute values of the negative pressure in the opening are significantly increased. The minimum negative pressure at the upper opening appears on the bottom of the leading edge of the opening, while the minimum negative pressure at the lower opening appears on the top of the leading edge of the opening. This phenomenon should be paid attention to by the structural designers.

Figure 9 illustrates the mean wind pressure distributions on side faces at different elevations for L-1 model, L-2 model, and L-3 model under wind direction of 0°, respectively. For L-1 model, it can be found that the flow around side faces is mainly separated. The minimum negative pressure appears on the side faces. For L-2 model, the area with a wind pressure coefficient of −0.7 at the top of the building is enlarged, while the area with a mean wind pressure coefficient of −0.65 and −0.6 near the upper and lower openings is reduced. By continuing to add the opening of the y-direction, it can be found that the area with a mean wind pressure coefficient of −0.7 at the upper opening and the area with a mean wind pressure coefficient of −0.6 at the lower opening are further reduced. There are two reasons for this phenomenon. On the one hand, the opening on the windward face reduces the flow energy of vorticities, resulting in the reduction of wind pressure on the side surface. On the other hand, the opening on the y-direction changes the flow field characteristics near the opening. The uniform vertical mixing component caused by the vortex on the original building surface and flow in the side opening strikes the upper side of the opening, which together cause a significant reduction in the negative pressure (absolute value) above the opening.

2.3. Wind Speed Amplification Effect of Upper and Lower Openings. The relationship between wind energy and wind speed is defined as follows:

$$P_w = \frac{1}{2}\rho A V^3, \tag{1}$$

where P_w is the power of the wind, ρ is the air density (kg/m^3), A is the swept area of rotor (m^2), and V is the mean wind speed (m/s) of incoming flow. It can be observed that the wind energy is proportional to the cube of the wind speed. The wind speed ratio R is introduced to describe the amplification effect of the mean wind speed in the opening:

$$R = \frac{V}{V_0}, \tag{2}$$

in which V is the mean speed in the direction of the axis of the opening and V_0 is the reference wind speed of an approaching location away from the model at the same height.

The numerical simulation can obtain the wind speed ratio at any position. The reference wind speeds are 7.75 m/s at 0.85 H and 7.16 m/s at 0.51 H, respectively. The reference wind speeds in the large opening models keep the same as those in the small opening models.

Tables 1 and 2 present the wind speed ratios of a_1–a_{11} monitoring points of the L-3 model and S-1 model under the wind direction of 0°, respectively. For L-3 model, all the wind speed ratios are larger than 1.0, indicating that all the wind speeds have been amplified in the opening. Moreover, the wind speed ratios firstly increase and then decrease along with the opening. The bold values in Tables 1 and 2 represent the maximum wind speed ratios for upper opening and lower opening, respectively. The maximum wind speed ratio occurs at a_3 point. The variation of wind speed ratios along with the opening in the lower opening keeps the same as that in the upper opening. The wind speed ratios in the lower opening are larger than those in the upper opening, implying that the

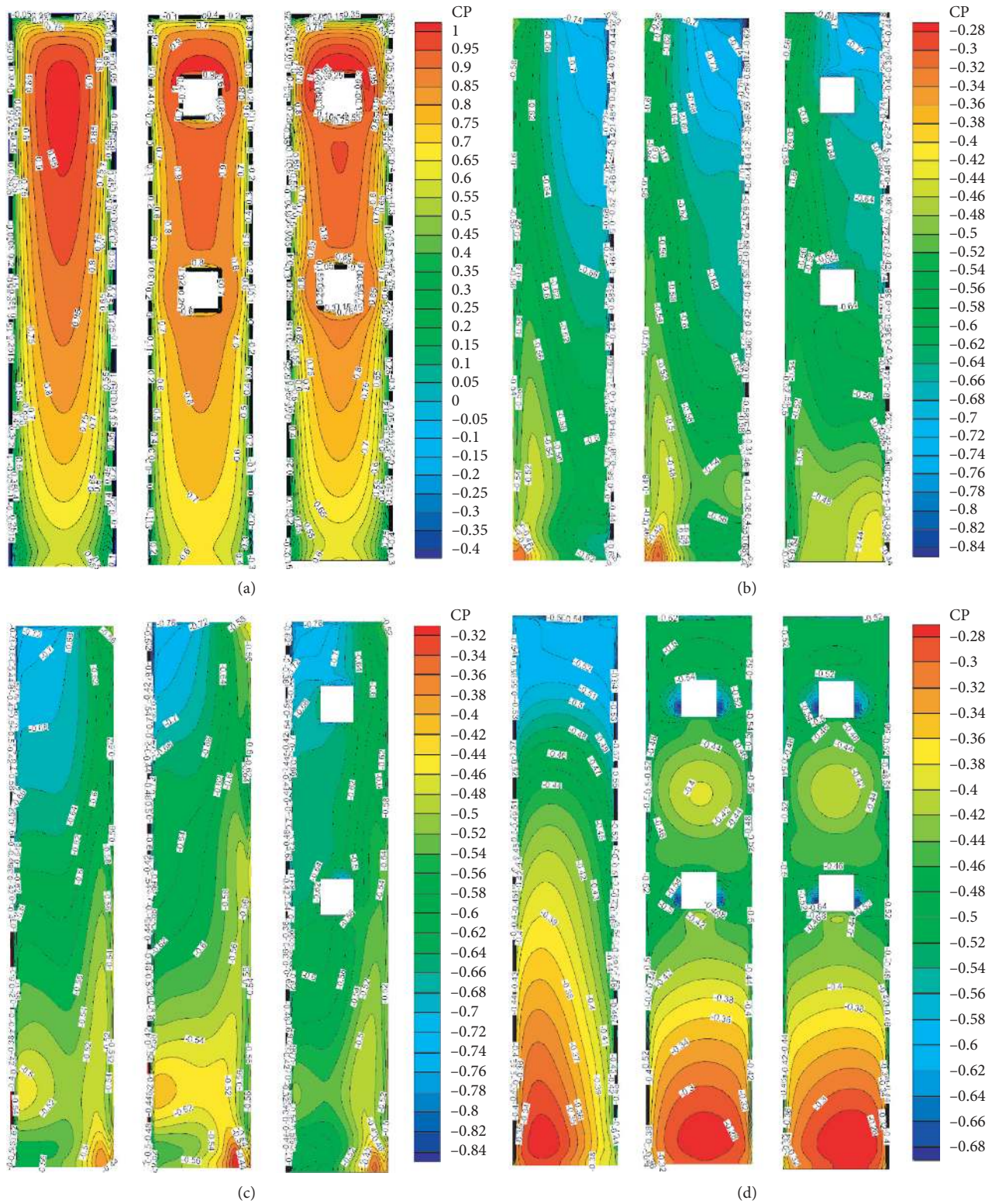

Figure 4: Mean wind pressure coefficients under wind direction of 0°. (a) Windward faces (from left to right, L-1, L-2, and L-3, the same below). (b) Left-side faces. (c) Right-side faces. (d) Leeward faces.

opening position is important for wind speed amplification. For S-1 model, the wind speed ratios are larger than 1.0 from monitoring points a_2 to a_6. The variation of wind speed ratios with the position of monitoring point keeps the same pattern with that in L-3 model. The maximum wind speed ratio occurs at a_2 point.

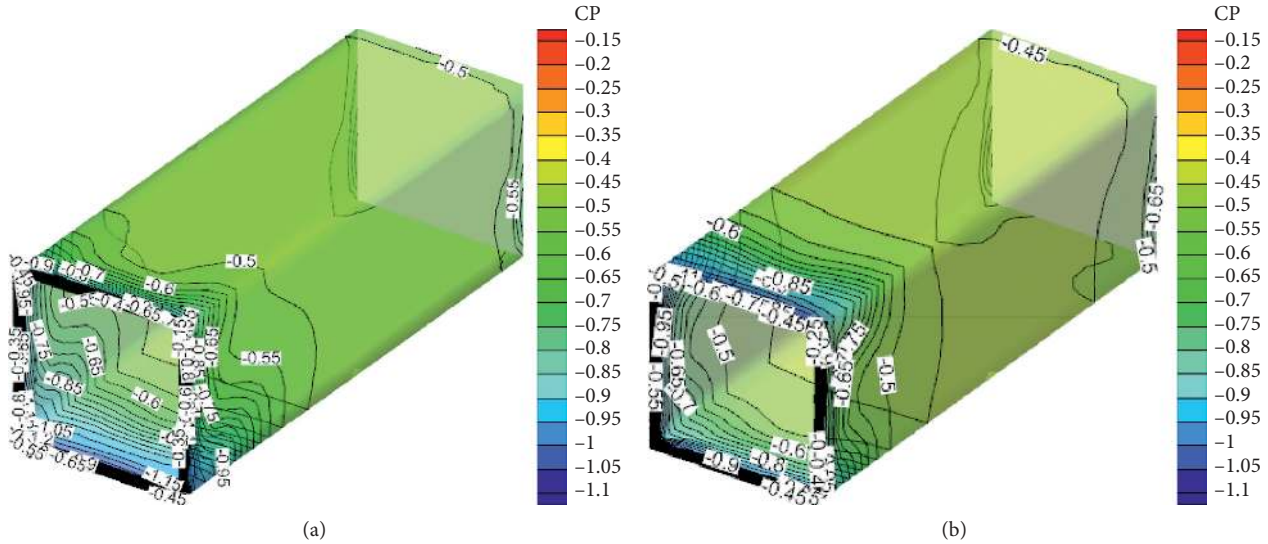

Figure 5: Mean wind pressure distribution in the openings of L-2 model. (a) Upper opening. (b) Lower opening.

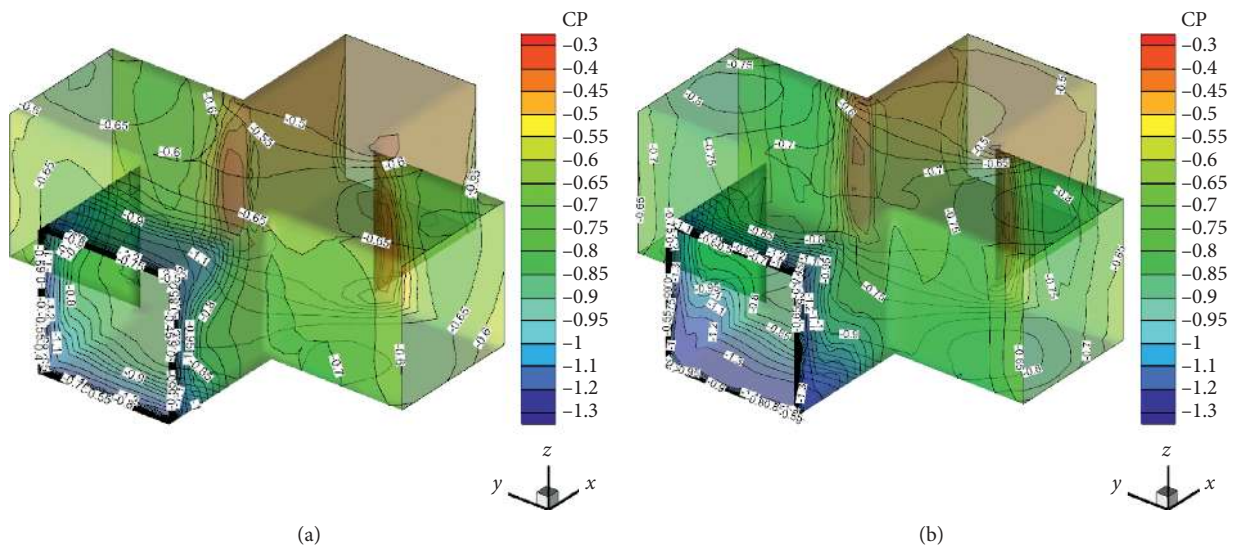

Figure 6: Mean wind pressure distribution in the openings of L-3 model. (a) Upper opening. (b) Lower opening.

2.4. The Variation of Flow Field with Wind Direction. Tables 3 and 4 illustrate the variation of wind speed of monitoring points b_1 and b_{11} on the L-3 model with the wind direction, respectively. It can be seen that due to the influence of openings the wind velocities in the direction of parallel and vertical entrances at the side center point vary with the wind direction. For example, the wind speed in the y-direction of the b_{11} point is increased from the negative value (downward) with the increase of the wind direction. The separation bubble and the incoming flow separating the corners are directly introduced into the opening, and the airflow is introduced and discharged to change the original flow field. The streamlined diagram of wind speed from 0° to 45° shows the same pattern. The vortices of the side faces are clearly separated to form several smaller vortices, indicating that the frequency of vortex shedding is also reduced.

3. Wind Tunnel Test

According to the influence of surface distribution on wind, the surface roughness is divided into four different categories: A, B, C, and D [25]. The model and wind field simulated in the wind tunnel are shown in Figure 10. The mean wind velocity profile and turbulence intensity of the terrain B are simulated. This terrain type specifies a mean wind speed profile with a power law exponent of $\alpha = 0.22$. The wind tunnel geometric scale ratio is 1:300.

The 1:300 scaled model corresponds to the actual structure dimension with length, width, and height of

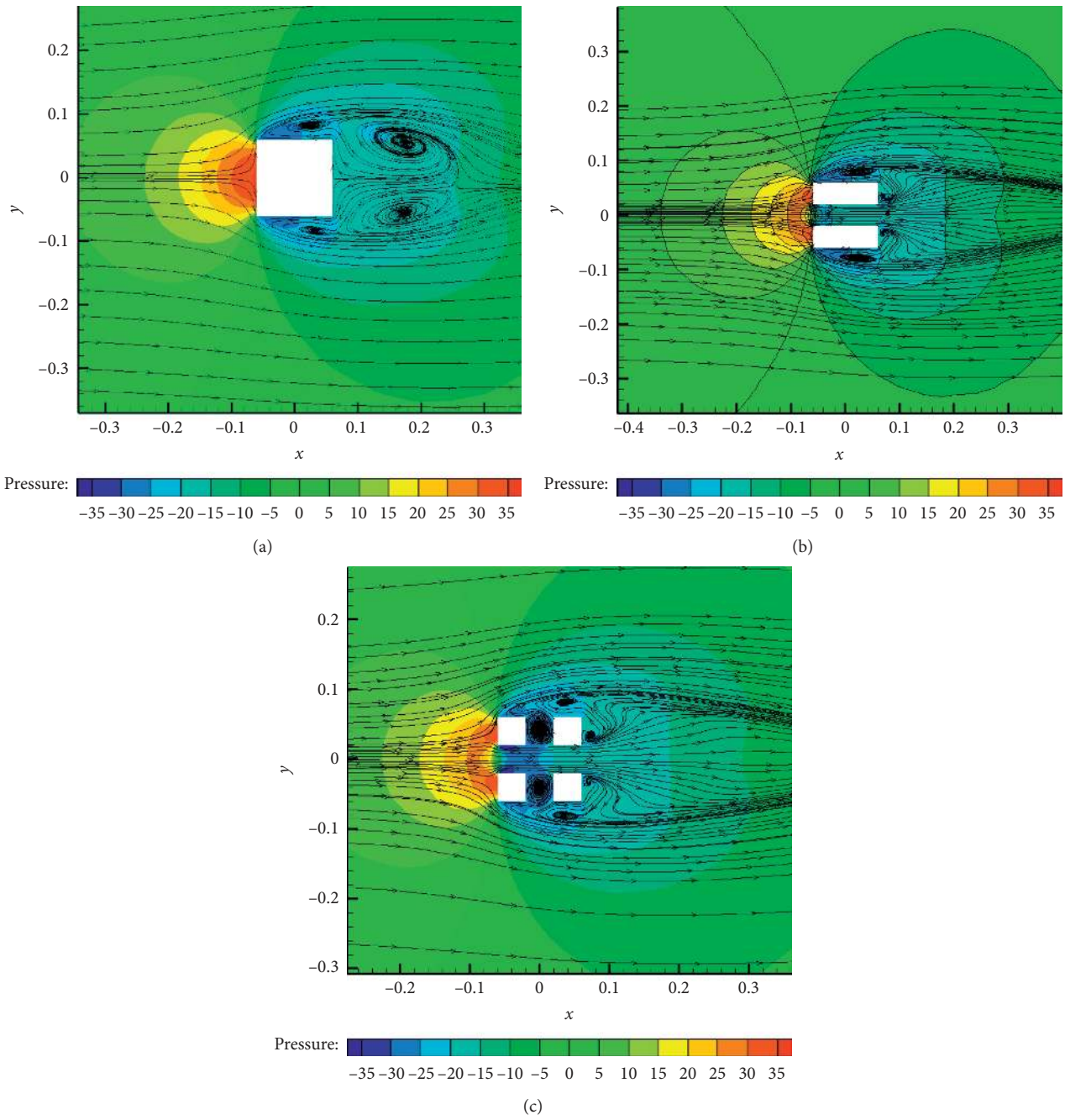

Figure 7: Mean wind pressure contour distributions with streamlines at height of 0.85 H. (a) L-1 model. (b) L-2 model. (c) L-3 model.

36 m × 36 m × 180 m. The model has openings in four surfaces at the heights of 0.5 H and 0.85 H, and the openings run through the wall and are connected with each other. Two models with different opening rates were made: model M-1 has a larger opening with a size of 12 m × 12 m; model M-2 has a smaller opening with a size of 6 m × 6 m. The ratio of section area of single opening to the area of the facade is defined as opening rate. The opening rates of larger opening and smaller opening are 2.22% and 1.11%, respectively. In each model, there are 22 measurement layers and totally 512 measuring points, of which layers H, J, K, T, U, and V are 32 measuring points in each layer. The remaining 16 layers are the standard measuring layer, and each standard layer has 20 measuring points. Detailed descriptions of the model façade and measurement points are shown in Figures 11 and 12.

The wind pressure coefficient in this study is expressed by the incoming wind pressure at the height of the building top (180 m) as the reference wind pressure. The expression is defined as follows:

$$C_{pi}(t) = \frac{p_i(t) - p_0}{(1/2)\rho V_H^2}, \tag{3}$$

where $C_{pi}(t)$ is the wind pressure coefficient time history of a certain measurement point i on the model; $p_i(t)$ is the wind pressure value of the single-sided measuring point i on the

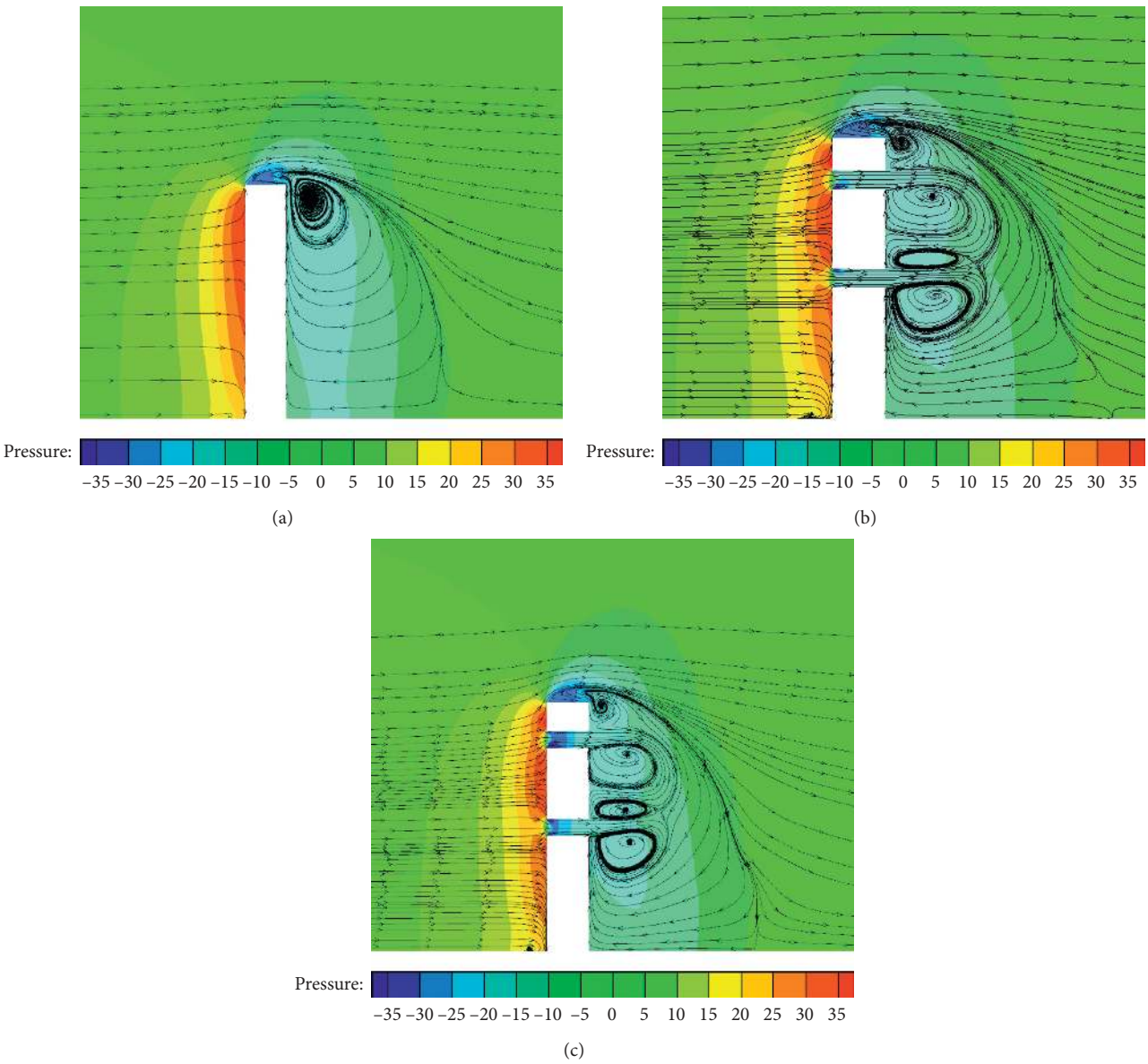

Figure 8: Mean wind pressure distributions on windward and leeward faces at different elevations. (a) L-1 model. (b) L-2 model. (c) L-3 model.

model; p_0 is the static pressure; V_H is the mean wind speed at the reference height; and ρ is air density and equals 1.25 kg/m^3.

After the time history of the wind pressure coefficient is recorded, the mean wind pressure coefficient and the standard deviation of the fluctuating wind pressure can be obtained by the following equations:

$$C_{\text{pmean}} = \frac{\sum_{k=1}^{N} C_{\text{pik}}(t)}{N}, \tag{4}$$

$$C_{\text{prms}} = \sqrt{\sum_{k=1}^{N} \frac{\left(C_{\text{pik}}(t) - C_{\text{pmean}}\right)}{(N-1)}}, \tag{5}$$

where C_{pmean} is the mean wind pressure coefficient of the pressure measuring point i, C_{prms} is the standard deviation of the fluctuating wind pressure, and N is the number of samples of the measuring point and equals 10,000 in the wind tunnel test.

3.1. Distribution Characteristics of Wind Pressure Coefficient on the Façade and Inner Wall of the Opening. In order to further discuss the wind pressure distribution, the inner wall of the opening is unfolded along the axis and named as A, B, C, and D faces, respectively, as shown in Figure 13. The mean wind pressure coefficient and fluctuating wind pressure coefficient distributions of different façades and different inner walls in the L-1, L-2, and L-3 model wind direction of 0° are presented in Figures 14 and 15. After analysis, the following conclusions can be drawn:

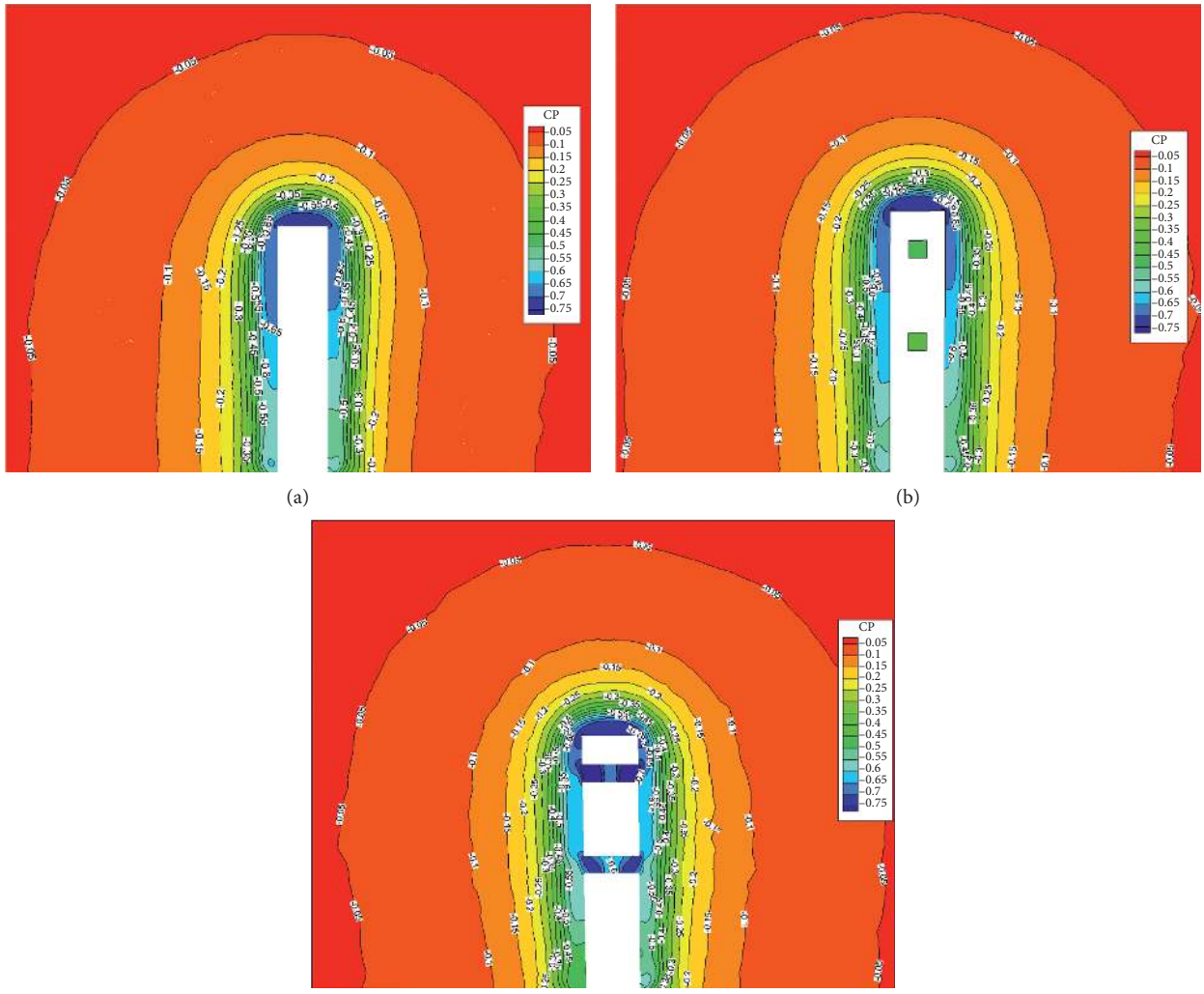

Figure 9: Mean wind pressure distributions on side faces at different elevations. (a) L-1 model. (b) L-2 model. (c) L-3 model.

(1) The mean wind pressure coefficients on the windward surface of L-1, L-2, and L-3 models are all positive. With the increase of height, the positive pressures increase and reach their maximum in the middle and upper altitude and then decrease owing to the three-dimensional flow around the top of model. For L-2 model with x-direction opening, the wind pressure coefficients change near the opening. The wind pressure coefficients near the upper and lower openings decrease slightly. For L-3 model with both x- and y-direction openings, the mean wind pressure distribution on the windward surface is almost the same as that in L-2 model. The fluctuating wind pressure on the windward surface gradually increases along the height for L-1 model. The overall variation of fluctuating wind pressure with opening is very small.

(2) Due to the horseshoe vortex phenomenon, the mean wind pressure coefficients on the side faces tend to be uniform along the height for L-1 model. The L-3 model can change the flow field characteristics of the side faces on the basis of L-2 and further reduce the mean and fluctuating wind pressure on the side faces. The fluctuating wind pressure coefficients of side faces change substantially uniformly along the height but gradually increase along the incoming flow direction. However, the fluctuating wind pressure coefficients are significantly reduced at the opening position.

(3) For L-1 model, the mean wind pressure coefficients on the leeward surface are negative. The wind pressure coefficients reach their maximum value at the bottom of model and increase in the circumferential direction. Once the opening is set, the mean and fluctuating wind pressure coefficients keep increasing from the inside to the outside along the circumferential direction. The fluctuating wind pressure coefficients on the leeward surface are

Figure 10: Model in the wind tunnel.

obviously increased, which needs to be paid more attention to.

(4) The mean and fluctuating wind pressure coefficients of inner wall AB and wall CD in both x-direction and y-direction are illustrated from Figures 16–19. It can be found that all the mean internal pressure coefficients of the opening wall are negative. The absolute value of the negative pressure coefficient at the front of the opening in x-direction is the largest and decreases rapidly along the flow approaching direction. The minimum negative pressure of the building appears at the front of the openings in the model of L-3. The distribution law of the fluctuating wind pressure keeps the same as the law of the mean wind pressure distribution. The fluctuating wind pressure coefficients reach its maximum value at the leading edge of the opening but decrease rapidly along the flow approaching direction and then become steady. The distribution of fluctuating wind pressure coefficients on the wall CD in the y-direction is different. Due to the influence of accelerated flow in the opening, the maximum fluctuating wind pressure coefficient appears near the middle opening and its value can reach 0.44. The fluctuating wind pressure coefficients on the wall of D decreases gradually from inside to outside along the circumferential direction. The fluctuating wind pressure on the surface C decreases gradually along the height.

3.2. Analysis of Wind Pressure Coefficients of Typical Measuring Layers. The mean wind pressure coefficients are quantitatively analyzed by taking the typical measurement layers of the large and small openings model. Among them, layer P is the measurement layer far from the openings, layer S is the measurement layer under the upper opening, and layer W is the measurement layer above the upper opening. Figure 20 presents the mean and fluctuating wind pressure coefficients of all measurement points in P, S, and W measurement layers near the upper opening of models L-1, L-2, and L-3 at the wind direction of 0°.

It can be found that the mean wind pressure coefficients of the windward surface measurement points increase after the openings are set. Compared with the S and W layers near the opening, the mean wind pressure coefficients on the windward surface of P layer increase slightly. The mean wind pressure coefficients in both side faces and leeward surfaces in L-2 and L-3 models are smaller than those in L-1 model. Moreover, the mean and fluctuating wind pressure coefficients in L-3 model are smaller than those in L-2 model, indicating that the mean wind pressure coefficients decrease dramatically in the model L-3 than in the model L-2.

3.3. The Variation of Wind Pressure Distribution of Typical Measuring Layers with Wind Direction. The typical measuring layers S and T at the heights of 0.81 H and 0.825 H are selected as the research objects to investigate the variation of the wind pressure coefficients of the measuring points with wind direction. Figure 21 shows the variation of the mean and fluctuating wind pressure coefficients of the measuring layers S with the wind direction. In the direction of the incoming flow, the measuring points on each façade are divided into an upwind direction and a downwind direction. For example, at 0° wind direction, the measuring points of S1–S2 are at the upwind direction while the measuring points of S4–S5 are at the downwind direction. By analyzing Figure 21, the following conclusions can be obtained:

(1) For the model L-1, as the wind direction increases, the absolute value of the mean wind pressure for measuring points S1–S5 first increases and then decreases. The maximum negative pressure occurs near the wind direction of 10°. At the measurement points of the downwind direction, the absolute value of the mean wind pressure decreases as the wind direction increases. After openings are set in the model L-3, the mean wind pressure values of the measuring points S1 and S5 are slightly reduced. Measuring points S2 and S3 on both sides of the opening are most affected. Compared with the fully enclosed L-1 model, the absolute value of negative pressure and positive pressure decrease at the same wind direction. As for the influence of the opening on the fluctuating wind pressure, it can be observed that although the S1–S5 measuring points of the L-1 model have some undulations, the fluctuating wind

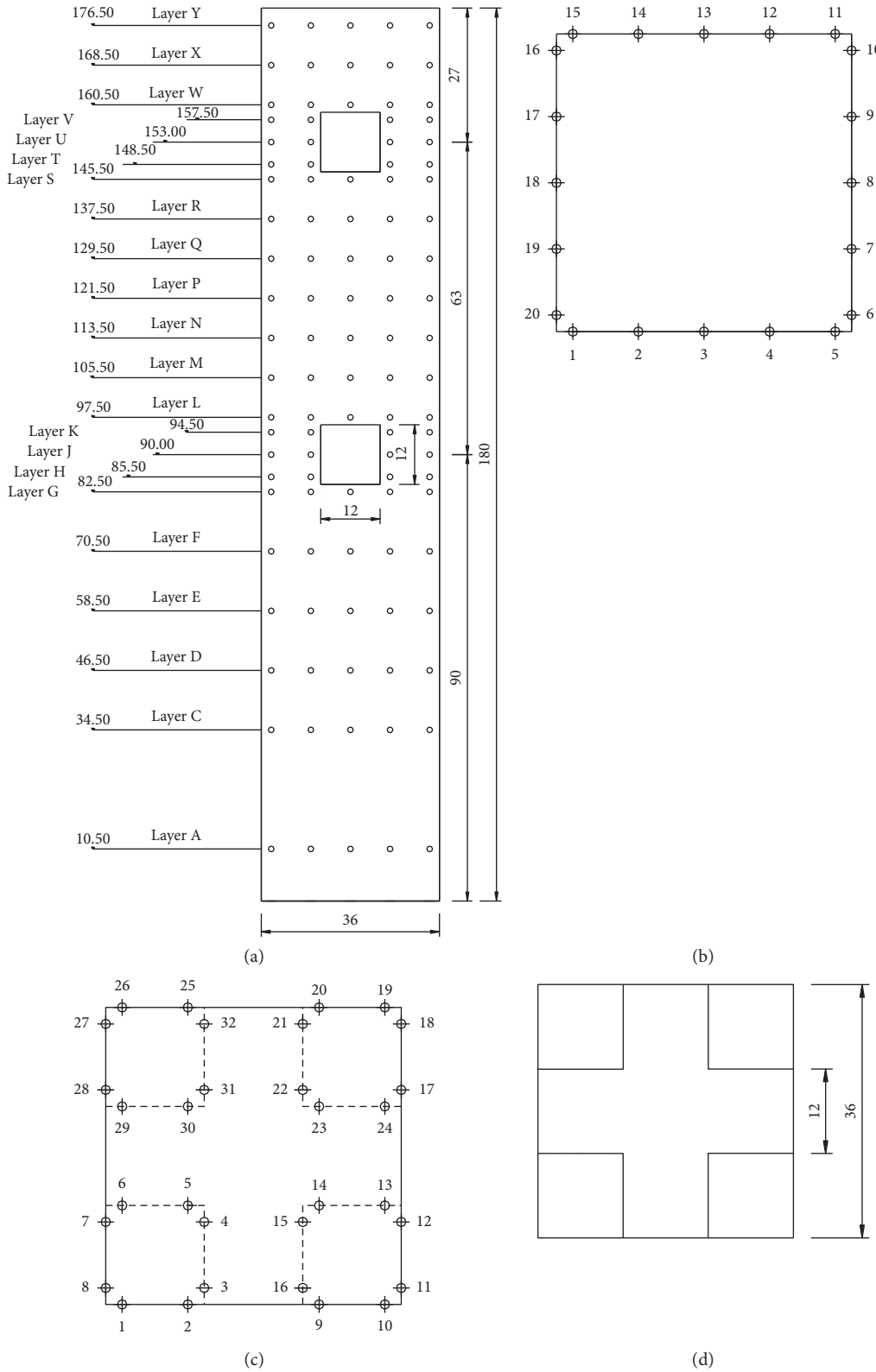

Figure 11: Continued.

(e)

Figure 11: Layout of measuring points for large opening model. (a) Layout of measuring points on facade. (b) Layout of measuring points on standard layer. (c) Layout of measuring points on the opening layer. (d) Dimensions of large openings. (e) Cross dimensions.

Table 1: Wind speed ratios of a_1–a_{11} monitoring points of the L-3 model under the wind direction of 0°.

Monitoring point	a_1	a_2	a_3	a_4	a_5	a_6	a_7	a_8	a_9	a_{10}	a_{11}
Upper opening	1.03	1.31	**1.35**	1.32	1.29	1.26	1.21	1.18	1.16	1.14	1.13
Lower opening	1.05	1.35	**1.38**	1.35	1.32	1.29	1.25	1.21	1.20	1.18	1.16

The bold values represent the maximum wind speed ratios for upper opening and lower opening, respectively.

Table 2: Wind speed ratios of a_1–a_{11} monitoring points of the S-1 model under the wind direction of 0°.

Monitoring point	a_1	a_2	a_3	a_4	a_5	a_6	a_7	a_8	a_9	a_{10}	a_{11}
Upper opening	0.94	**1.23**	1.20	1.13	1.12	1.05	0.96	0.92	0.92	0.91	0.92
Lower opening	0.98	**1.27**	1.21	1.18	1.13	1.07	0.98	0.94	0.94	0.94	0.94

The bold values represent the maximum wind speed ratios for upper opening and lower opening, respectively.

Table 3: Variation of wind speed of monitoring point b_1 on the L-3 model with wind direction (m/s).

Wind direction	0°	5°	10°	15°	20°	25°	30°	35°	40°	45°
V_X	−2.09	−1.96	−1.49	−0.63	−0.40	0.00	0.28	0.76	1.26	2.05
V_Y	0.62	0.08	−0.22	−0.15	−0.07	0.47	0.64	0.96	1.35	2.05

Table 4: Variation of wind speed of monitoring point b_{11} on the L-3 model with wind direction (m/s).

Wind direction	0°	5°	10°	15°	20°	25°	30°	35°	40°	45°
V_X	−2.09	−1.46	−1.58	1.16	3.64	4.62	4.63	4.46	4.01	3.54
V_Y	−0.57	−0.10	0.70	0.04	1.06	1.65	2.10	2.65	3.11	3.54

pressure generally increases and then decreases. The position of the maximum fluctuating wind pressure gradually moves from the downwind direction to the upwind direction as the wind direction increases, which also indicates that the position with the strongest turbulence action moves to upwind direction with the change of wind direction. After openings are set, it can be clearly seen that this variation has not been changed. The fluctuating wind pressure coefficients of all the measuring points are significantly reduced. The measuring points S1 and S5 at the edge are obviously reduced at the wind direction of 0°~15°. The maximum reduction of S1 at the wind direction of 0° is up to 25%. The fluctuating wind pressure coefficients of the measurement points S2 and S3 are reduced at all wind directions. The maximum reduction and the occurrence angles were 27% for 30° and 16% for 0°, respectively.

(2) For the L-3 model, the measuring points S6–S10 are transferred from the leeward surface to the side surface as the wind direction increases. The absolute value of the negative pressure of the measured points increases with the increase of wind direction. After the openings are set, the absolute value of negative pressure decreases greatly. The maximum reduction of S6–S10 occurs at the wind direction of 0°, and the maximum reduction is 16%, 18%, 26%, 20%, and 21%, respectively. The fluctuating wind pressure gradually decreases with the increase of the wind direction; the variation remains unchanged after the openings are set. The fluctuating wind pressure decreases greatly under the same wind direction.

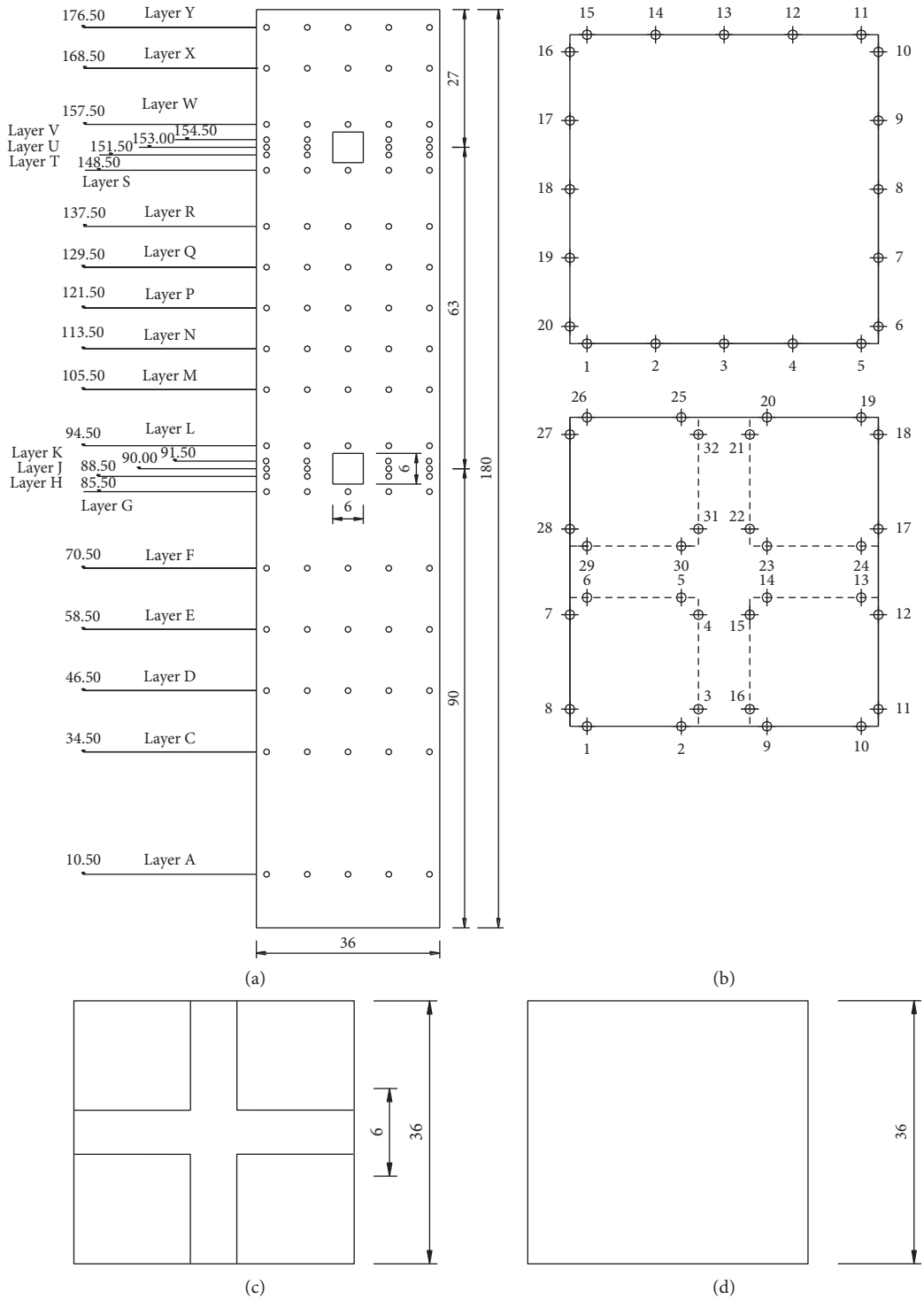

Figure 12: Layout of measuring points and geometric parameters for small opening model. Layout of measuring points on standard layer. (a) Layout of measuring points on facade. (b) Layout of measuring points on the opening layer. (c) Dimensions of small openings. (d) Cross dimensions.

(3) The measuring points of S11–S15 of the L-1 model are transferred from the side surface to the leeward surface. As the wind direction increases, the absolute values of the negative pressures of the measuring points first decrease and then increase. After the openings are set, the regularity of the measured points on the side surface shows fluctuation, and the mutation occurred at the wind directions of 10° and

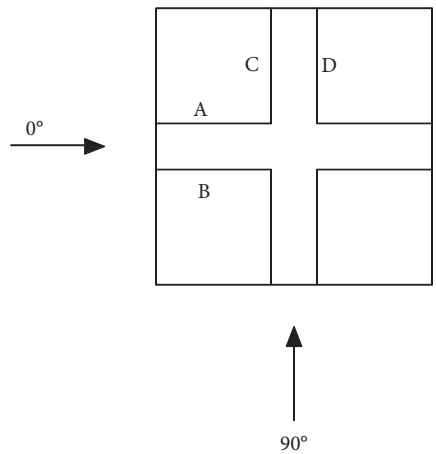

Figure 13: Schematic diagram of the inner wall of the opening.

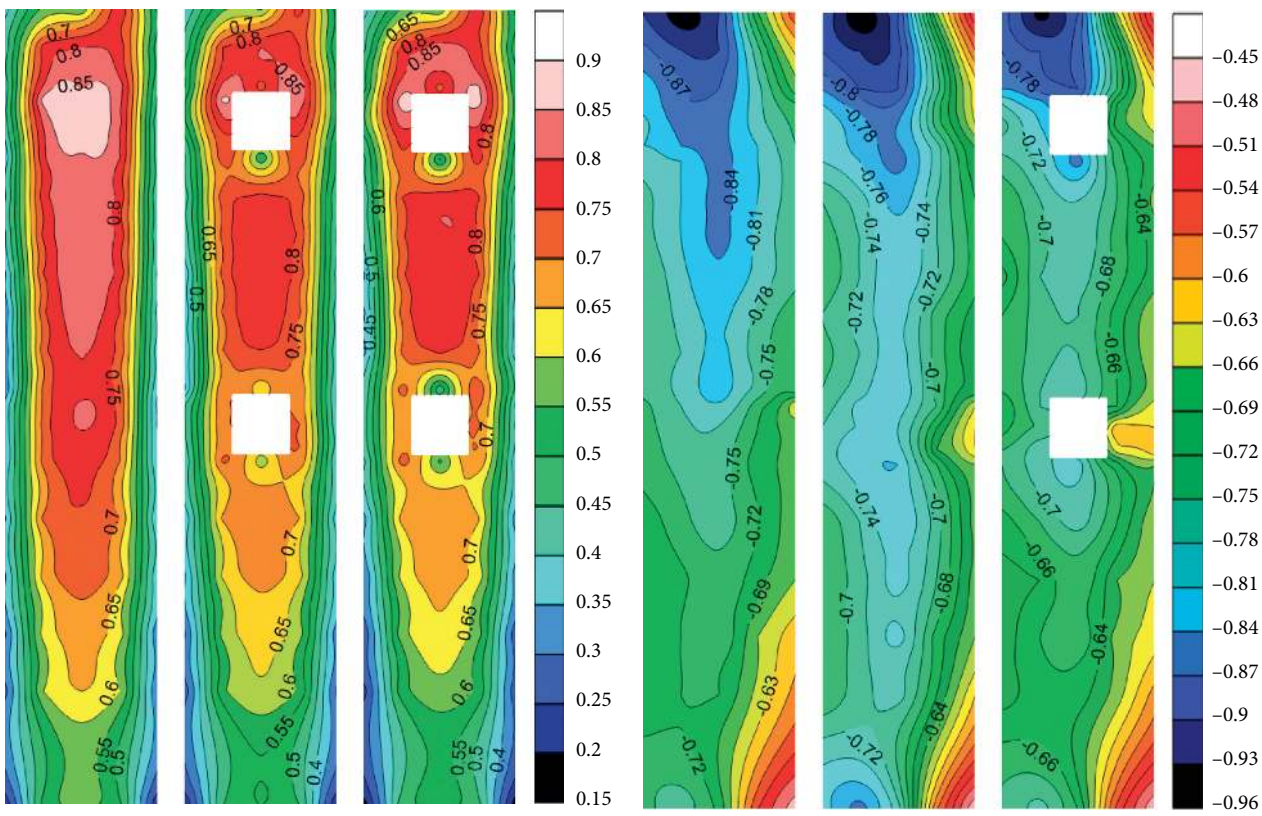

(a) (b)

Figure 14: Continued.

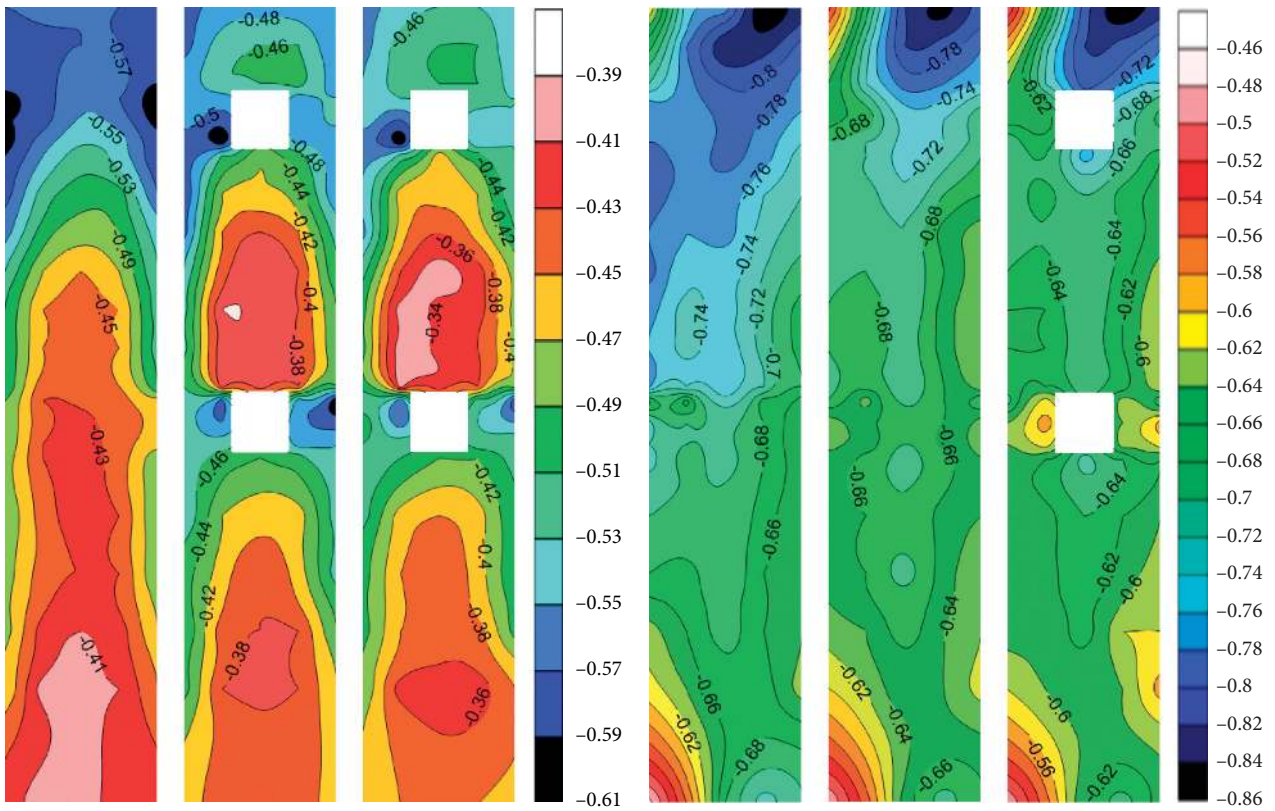

Figure 14: Distribution of mean wind pressure coefficients on the façades under the wind direction of 0°. (a) Windward surface (from left to right, L-1, L-2, and L-3, the same below). (b) Right-side wind surface. (c) Leeward surface. (d) Left-side wind surface.

25°. The absolute value of the negative pressure is greatly reduced. The maximum reductions of S11–S15 are all emerged at the wind directions of 45°, which is 19%, 19%, 23%, 19%, and 22%, respectively. The fluctuating wind pressure in the L-1 model decreases with the increasing of the wind direction. The variation remains unchanged after the openings are set. The amplitude decreases greatly within the wind direction range of 0°–15°.

(4) In the fully enclosed model L-1, the measuring points S16–S20 are transferred from the windward surface to the side surface as the wind direction increases. The positive pressure of the windward measuring point first increases and then decreases as the wind direction increases. The maximum positive pressure of the windward surface appears at the wind direction of 20° for the measuring point S19. The maximum positive pressure of the middle measuring point S18 appears at the wind direction of 5°. After the openings are set, the positive pressure increases at the wind direction of 0° of the measuring point in the upwind direction. The mean wind pressure coefficients are greatly reduced within the wind direction range of 0°–20° due to the influence of the openings. The fluctuating wind pressure of the measuring point of the L-1 model keeps decreasing as the wind direction increases, except for the upwind direction edge measuring point S20. After the opening is set, the variation of the fluctuating wind pressure coefficients with the wind direction keeps the same as before. The fluctuating wind pressure coefficients of the upwind direction measuring point increase and are larger than those of the L-1 model in many wind directions.

Figure 22 shows the variation of the mean and fluctuating wind pressure coefficients of the measuring layers T with the wind direction. Compared the results of the L-1 model with those of the L-3 model, it can be found that the windward surface of the measuring points T27-T8 is transferred to the side surface with the increase of the wind direction. The side surface of the measuring point T1-T10 is transferred to the leeward surface with the increase of wind direction. The variation of mean and fluctuating wind pressure coefficients with the wind direction is the same as that of layer S. The measuring points T19 and T26 are transferred from the side surface to the leeward surface as the wind direction increases. The mean negative pressures of measurement point T20 in downwind direction at some wind directions are greater than the maximum negative pressures at the side surface without openings. The measurement point T20 is in the downwind position and its fluctuating wind pressure increases obviously at the wind

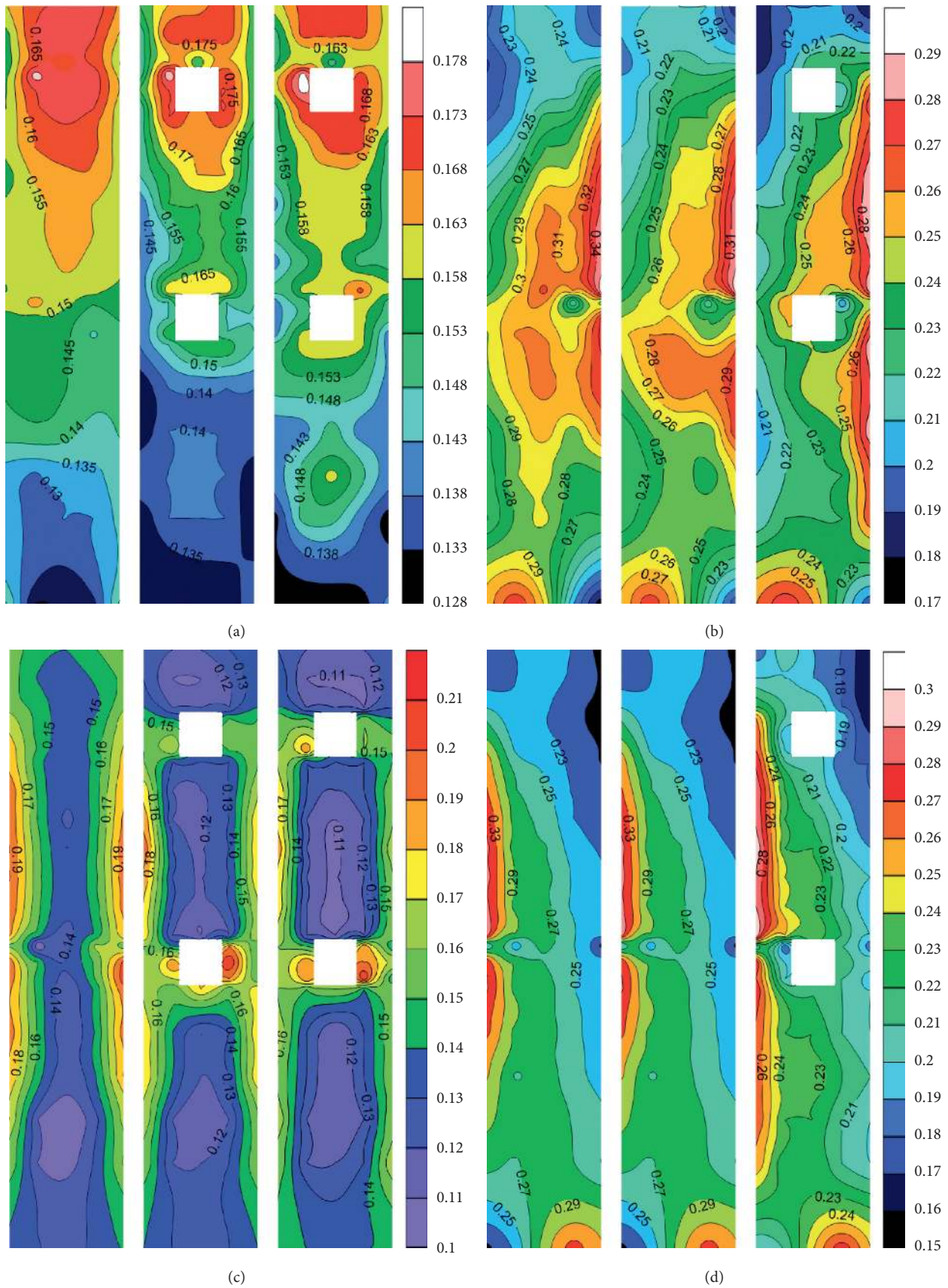

Figure 15: Distribution of fluctuating wind pressure coefficients on the façade under the wind direction of 0°. (a) Windward surface (from left to right, L-1, L-2, and L-3, the same below). (b) Right-side wind surface. (c) Leeward surface. (d) Left-side wind surface.

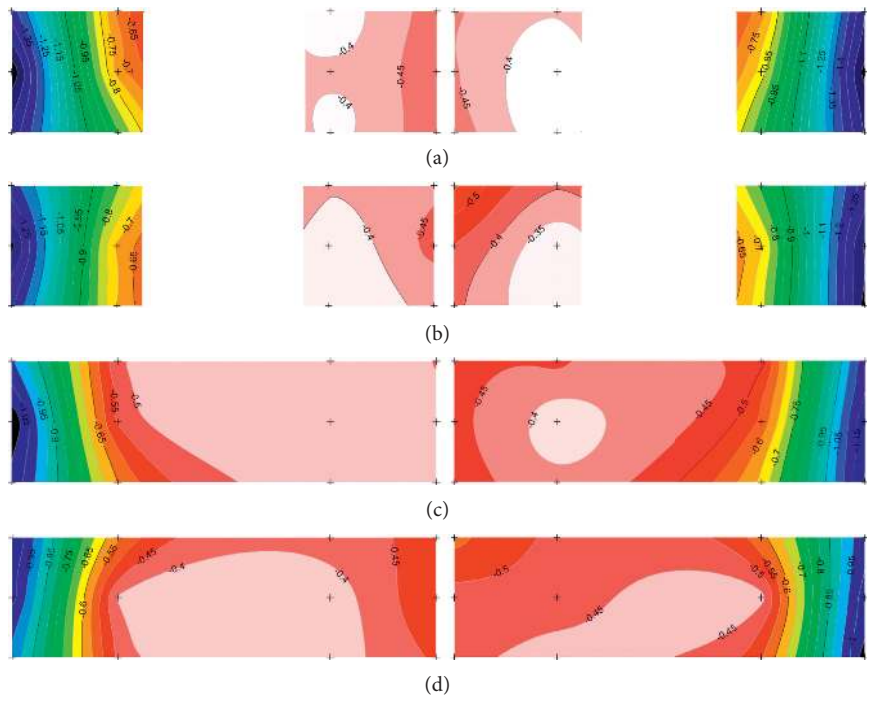

(a)

(b)

(c)

(d)

Figure 16: Mean wind pressure coefficients of wall AB in the x-direction. (a) Wall AB at the upper opening in the model of L-3 (expanding along the axis, the left side represents the A side (the flow flows from left to right); the right side represents the B side (the flow flows from right to left), the same below). (b) Wall AB at the lower opening in the model of L-3. (c) Wall AB at the upper opening in the model of L-2. (d) Wall AB at the lower opening in the model of L-2.

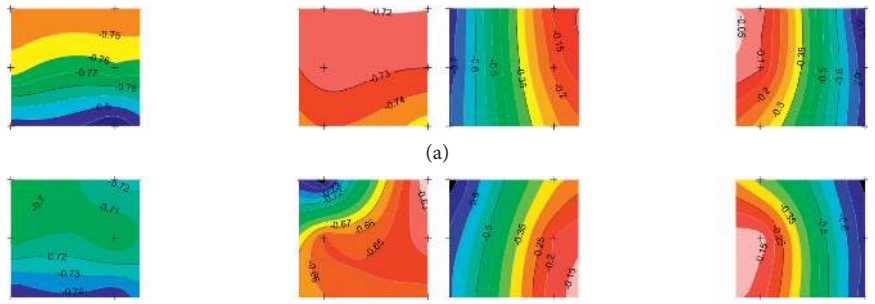

(a)

(b)

Figure 17: Mean wind pressure coefficients of wall CD in the y-direction. (a) Wall CD at the upper opening in the model of L-3 (expanding along the axis, the left side represents the C side (the flow flows from left to right); the right side represents the D side (the flow flows from right to left), the same below). (b) Wall CD at the lower opening in the model of L-3.

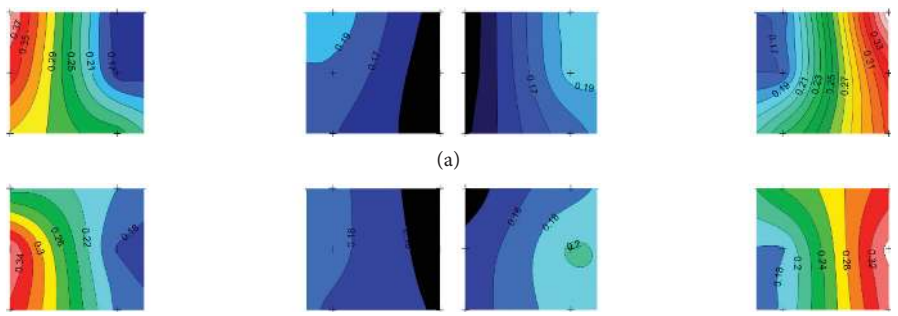

(a)

(b)

Figure 18: Continued.

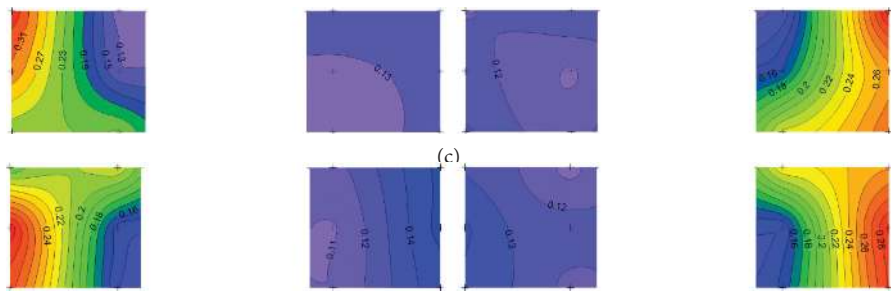

(c)

(d)

Figure 18: Fluctuating wind pressure coefficients of wall AB in the x-direction. (a) Wall AB at the upper opening in the model of L-3. (b) Wall AB at the lower opening in the model of L-3. (c) Wall AB at the upper opening in the model of L-2. (d) Wall AB at the lower opening in the model of L-2.

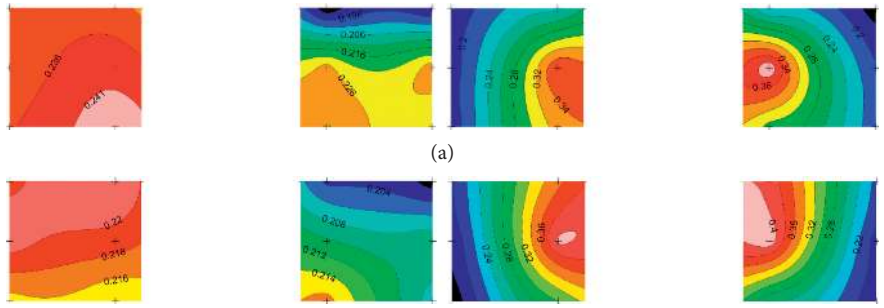

(a)

(b)

Figure 19: Fluctuating wind pressure coefficients of wall CD in the y-direction. (a) Wall CD at the upper opening in the model of L-3. (b) Wall CD at the lower opening in the model of L-3.

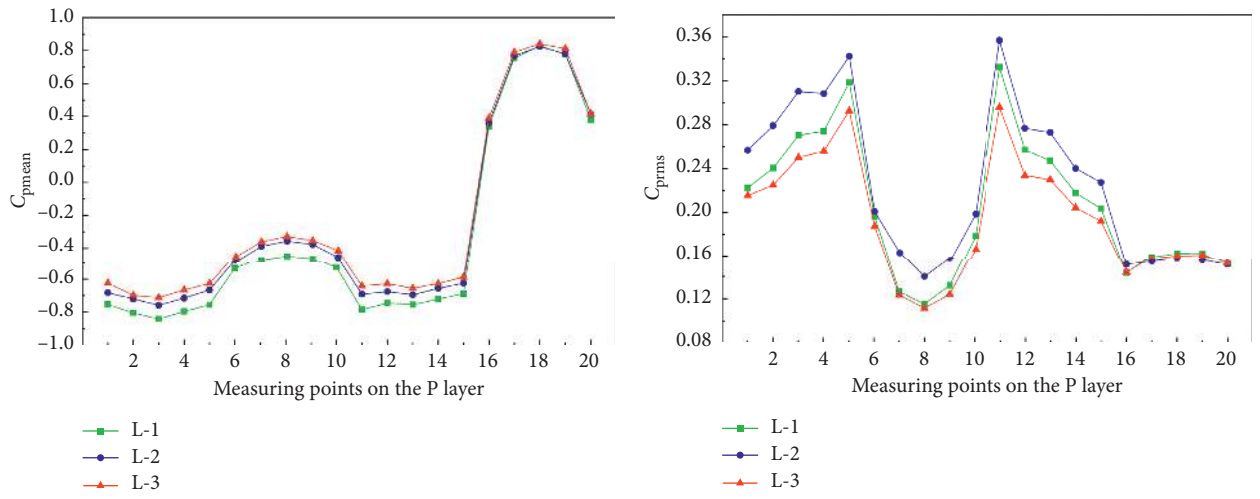

(a)

(b)

Figure 20: Continued.

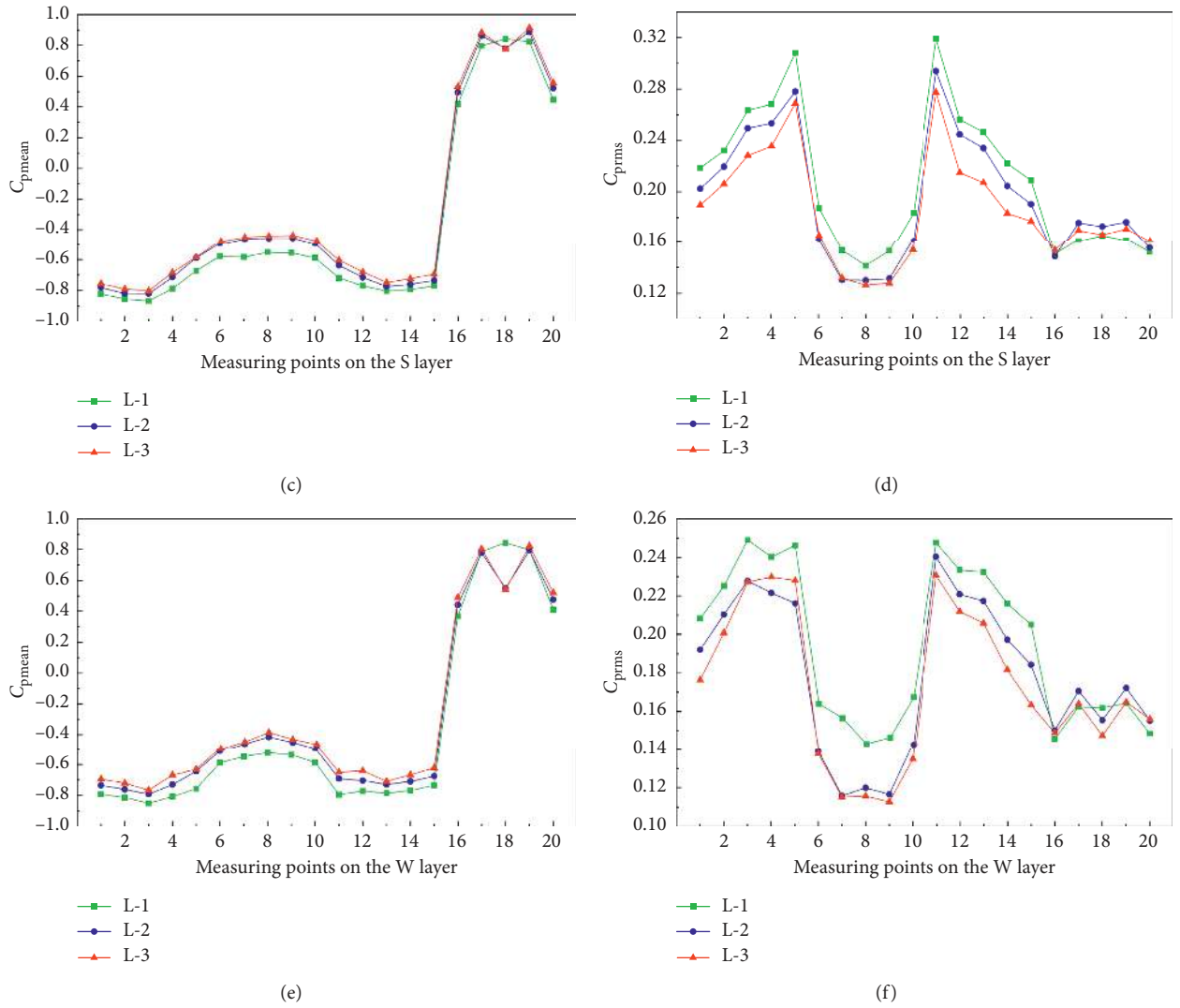

FIGURE 20: Mean wind pressure and fluctuating wind pressure distribution of typical measuring layers. (a) Mean pressure coefficients on layer P. (b) Fluctuating pressure coefficients on layer P. (c) Mean pressure coefficients on layer S. (d) Fluctuating pressure coefficients on layer S. (e) Mean pressure coefficients on layer W. (f) Fluctuating pressure coefficients on layer W.

direction of 45°, which is 39% higher than that of L-1 model. The measuring points T11 and T8 are transferred from the leeward surface to the side surface as the wind direction increases. T17 and T12 on both sides of the opening are affected by the opening. The absolute values of the mean wind pressure and the fluctuating wind pressure of T12 in the upwind direction within the wind direction range of 0°–20° after the opening are greatly increased when comparing to the unopened working condition. The mean negative pressures of T17 in the downwind direction at most wind directions are greater than negative pressures in the side surface of L-1 model. After the wind direction increases to 10°, the fluctuating wind pressure of measurement point T17 in the downwind position is significantly increased. At the wind direction of 28°, it increases by 28% compared with the fully enclosed condition.

3.4. Wind Speed Amplification Effects in the Openings. The wind speed amplification effects in the openings are studied for model with openings in x-direction and the model with openings in both x-direction and y-directions. Figures 23 and 24 show the variation of the wind speed ratio with the wind direction of the model with large and small openings. For the L-2 model with large openings, the wind speed ratio increases steadily with the increasing wind direction and reaches the maximum value between the wind direction range of 25°–35°, but then it decreases rapidly. The maximum wind speed ratio appears at an oblique angle with the incoming flow. This phenomenon is consistent with the conclusions of Li et al. [26] and Zhang et al. [27]. For the L-3 model, the wind direction corresponding to the maximum value of wind speed ratio changes, all of which occur at the wind direction of 0°. The wind speed ratio keeps steady

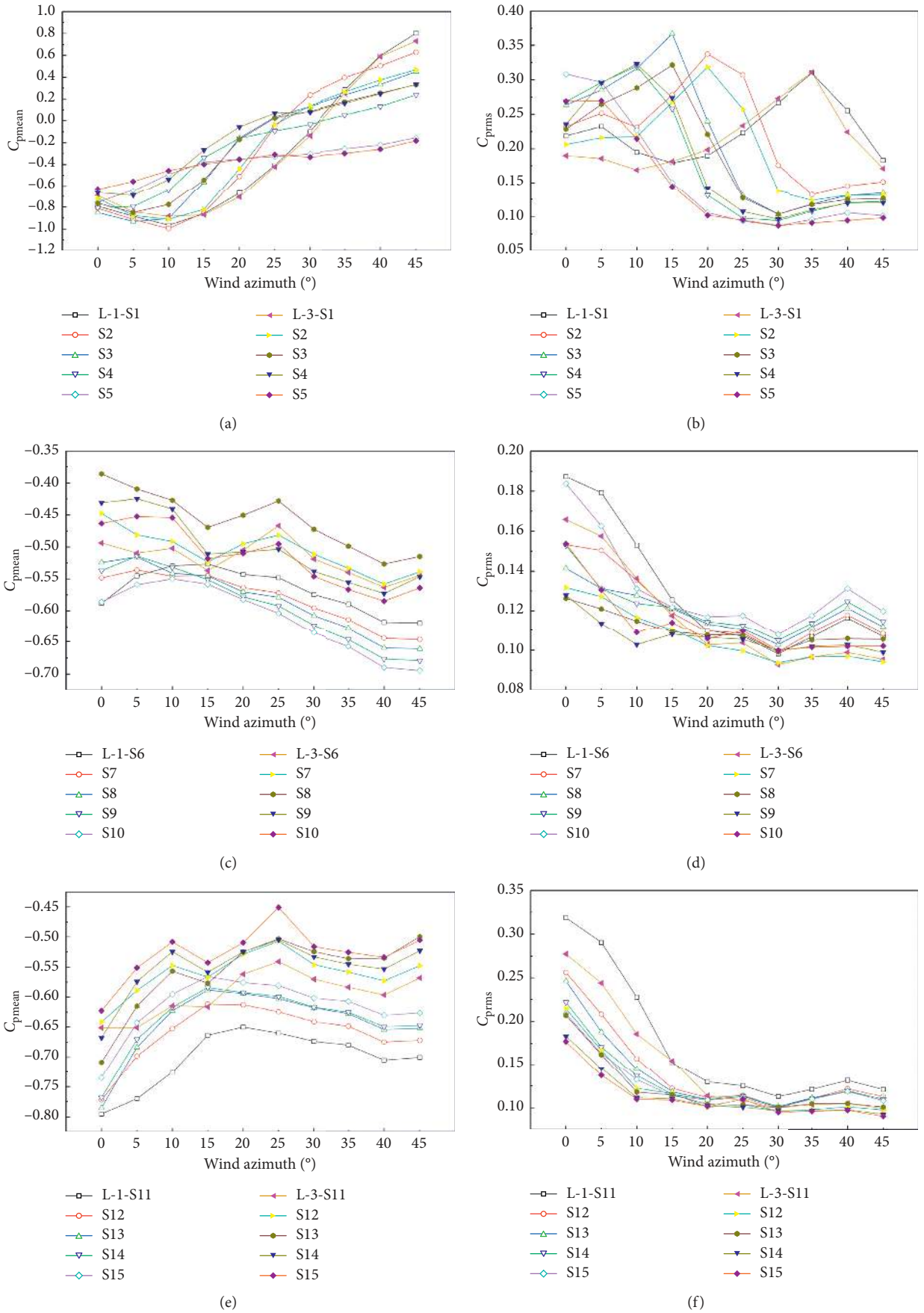

Figure 21: Continued.

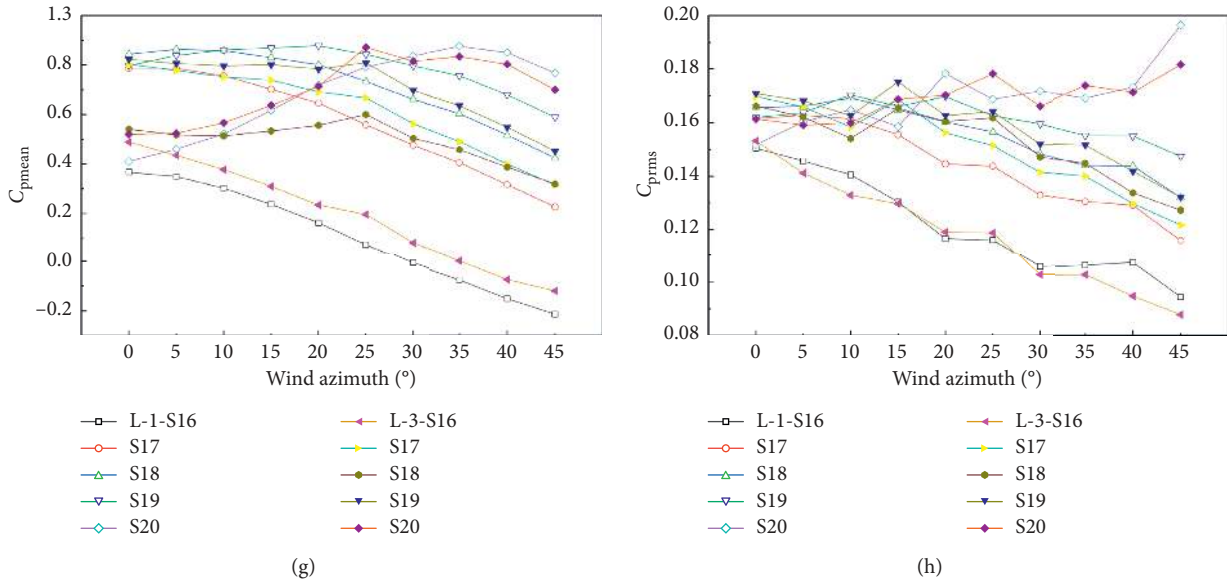

Figure 21: The variation of the mean and fluctuating pressure coefficients of the layer S in the models L-1 and L-3 with the wind direction. (a) Mean pressure coefficients (S1–S5). (b) Fluctuating pressure coefficients (S1–S5). (c) Mean pressure coefficients (S6–S10). (d) Fluctuating pressure coefficients (S6–S10). (e) Mean pressure coefficients (S11–S15). (f) Fluctuating pressure coefficients (S11–S15). (g) Mean pressure coefficients (S16–S20). (h) Fluctuating pressure coefficients (S16–S20).

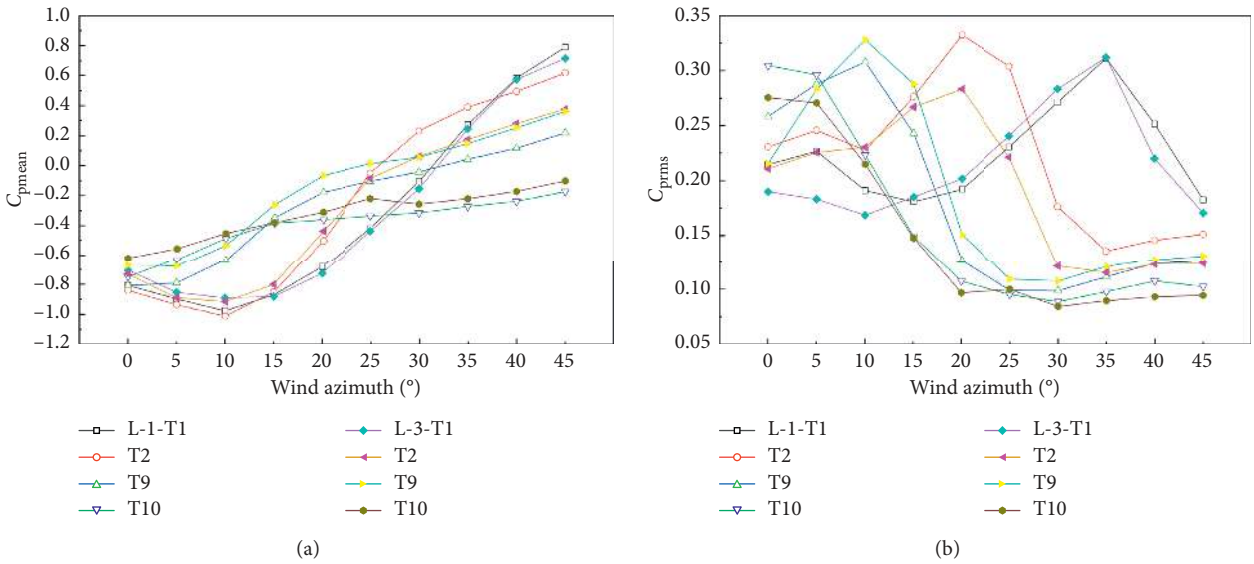

Figure 22: Continued.

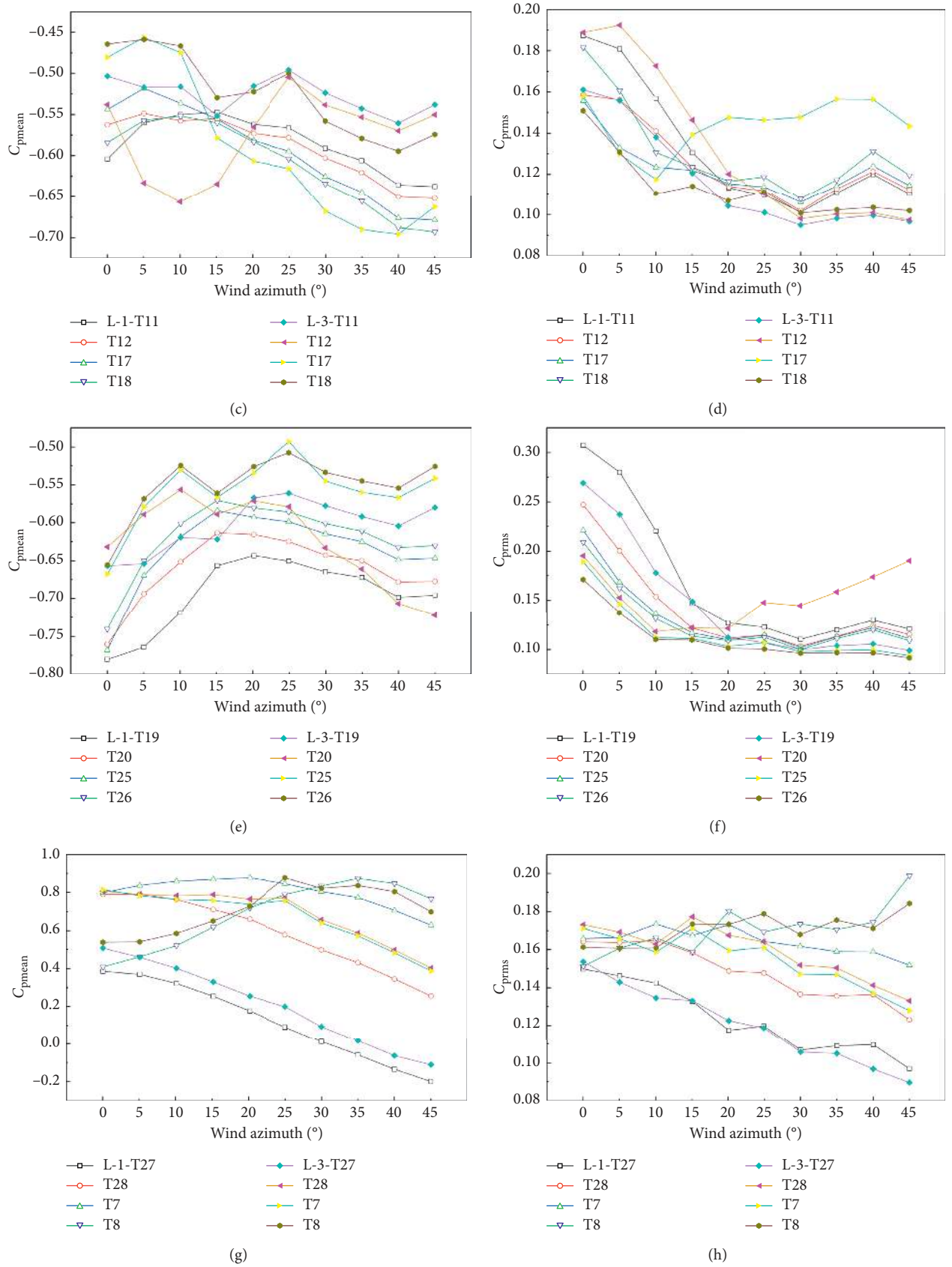

Figure 22: The variation of the mean and the fluctuating pressure coefficients of the T layer in the models of L-1 and L-3 with the wind direction. (a) Mean pressure coefficients (T1, T2, T9, and T10). (b) Fluctuating pressure coefficients (T1, T2, T9, and T10). (c) Mean pressure coefficients (T11, T12, T17, and T18). (d) Fluctuating pressure coefficients (T11, T12, T17, and T18). (e) Mean pressure coefficients (T19, T20, T25, and T26). (f) Fluctuating pressure coefficients (T19, T20, T25, and T26). (g) Mean pressure coefficients (T27, T28, T7, and T8). (h) Fluctuating pressure coefficients (T27, T28, T7, and T8).

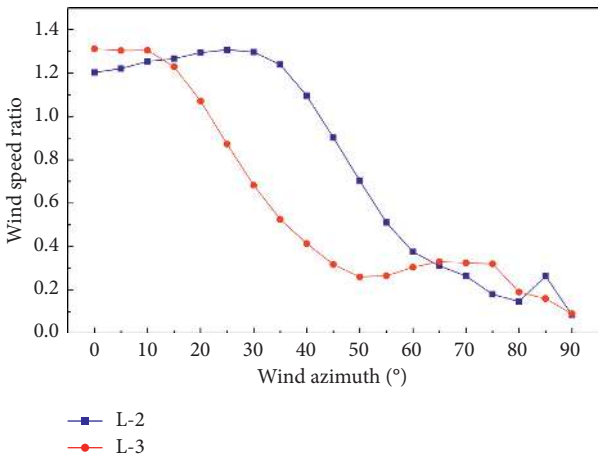

Figure 23: The variation of the wind speed ratio in the models of L-2 and L-3 with the wind direction.

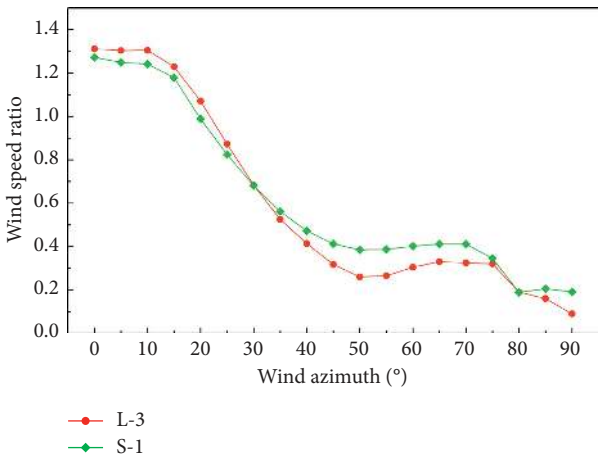

Figure 24: The variation of the wind speed ratio in the models of L-3 and S-1 with the wind direction.

between wind directions of 0°–15°. However, it decreases rapidly after exceeding wind direction of 15°. Setting openings in both x-direction and y-direction can obtain a larger wind speed ratio than that obtained from the model of openings only in x-direction between the wind direction range of 0°–10°. The wind speed ratio can be increased by 8.3% when the maximum value appears at the wind direction of 0° in the model with large openings and by 9.2% when the maximum value appears at the wind direction of 0° in the model with small openings. This shows that at a wind direction of 0°–10°, setting openings in both x-direction and y-direction can obtain a larger wind speed ratio than that with openings only in x-direction. The model L-2 can keep the wind speed ratio greater than 1.0 in the wind direction range of 0°–45°, while the model L-3 can obtain a larger wind speed ratio than that obtained from model L-2 in the range of 0°–10°. But the wind speed ratio decreases rapidly with the increase of wind direction. The wind speed ratio is less than 1.0 when wind direction exceeds 20°.

4. Conclusions

Based on numerical simulation and wind tunnel testing, this study investigated the wind loads and wind speed amplifications on high-rise buildings with openings. The main conclusions are listed as follows:

(1) The numerical simulation results of high-rise buildings with opening are almost consistent with those of wind tunnel study, showing good verification with each other.

(2) The wind pressure distribution on the high-rise building surfaces is changed after openings are set. Although the mean wind pressure coefficients of the windward surface increase at local position, they are reduced overall. Setting openings in both x-direction and y-direction can further reduce the mean and the fluctuating wind pressure coefficients compared to only setting openings in x-direction. However, the inner walls of the openings are subjected to larger negative pressure in the x-direction.

(3) For the large and small openings, the model L-2 with openings only in x-direction can maintain the wind speed ratio greater than 1.0 in the wind direction range of 0° 45°. The model L-3 can obtain a wind speed ratio of 8.3% 9.2% higher than that of model L-2 in the wind direction range of 0°–10° of the wind direction, indicating that wind energy can be utilized more effectively in high-rise buildings with opening in the x-direction.

(4) When the openings are set in x-direction, the airflow on the windward surface is introduced into the leeward surface, changing the flow field characteristics of the position of the original opening and the leeward surface. The openings in the y-direction can further change the flow field distribution. Compared with the model L-2, the vortex size in side surface is decreased and the peripheral wind speed is decreased.

(5) Once the openings are set, the single vortex from the top of the leeward surface is scattered and reduced to four vortexes of different sizes. The model L-3 produces a larger negative pressure in the opening compared to the model L-2. The extreme wind pressure values in the opening of the model L-2 appear on the bottom of the upper opening and the top of the lower opening respectively, indicating that the position of the opening has important influence on the wind load of high-rise building.

Data Availability

The data used to support the findings of this study are available from the corresponding author upon request.

Conflicts of Interest

The authors declare that they have no conflicts of interest regarding the publication of this paper.

Acknowledgments

This work was fully supported by the grants from the National Natural Science Foundation of China (project nos. 51778072, 51708207, and 51408062), a grant from Hunan Provincial Natural Science Foundation (project no. 2020JJ5176), and a grant from Hunan Provincial Education Department (project no. 18B206).

References

[1] A. Kareem, "Dynamic response of high-rise buildings to stochastic wind loads," *Journal of Wind Engineering and Industrial Aerodynamics*, vol. 42, no. 1–3, pp. 1101–1112, 1992.

[2] P. A. Irwin, "Wind engineering challenges of the new generation of super-tall buildings," *Journal of Wind Engineering and Industrial Aerodynamics*, vol. 97, no. 7-8, pp. 328–334, 2009.

[3] Y. Li and Q.-S. Li, "Wind-induced response based optimal design of irregular shaped tall buildings," *Journal of Wind Engineering and Industrial Aerodynamics*, vol. 155, pp. 197–207, 2016.

[4] Y. Li, Q. S. Li, and F. Chen, "Wind tunnel study of wind-induced torques on L-shaped tall buildings," *Journal of Wind Engineering and Industrial Aerodynamics*, vol. 167, pp. 41–50, 2017.

[5] M. Gu and Y. Quan, "Across-wind loads of typical tall buildings," *Journal of Wind Engineering and Industrial Aerodynamics*, vol. 92, no. 13, pp. 1147–1165, 2004.

[6] A. Kareem, "Mitigation of wind induced motion of tall buildings," *Journal of Wind Engineering and Industrial Aerodynamics*, vol. 11, no. 1–3, pp. 273–284, 1983.

[7] H. Tanaka, Y. Tamura, K. Ohtake, M. Nakai, and Y. Chul Kim, "Experimental investigation of aerodynamic forces and wind pressures acting on tall buildings with various unconventional configurations," *Journal of Wind Engineering and Industrial Aerodynamics*, vol. 107-108, pp. 179–191, 2012.

[8] A. Sharma, H. Mittal, and A. Gairola, "Mitigation of wind load on tall buildings through aerodynamic modifications: Review," *Journal of Building Engineering*, vol. 18, pp. 180–194, 2018.

[9] Y. Li, X. Tian, K. F. Tee, Q.-S. Li, and Y.-G. Li, "Aerodynamic treatments for reduction of wind loads on high-rise buildings," *Journal of Wind Engineering and Industrial Aerodynamics*, vol. 172, pp. 107–115, 2018.

[10] Y. Li, Y.-G. Li, Q.-S. Li, and K.-F. Tee, "Investigation of wind effect reduction on square high-rise buildings by corner modification," *Advances in Structural Engineering*, vol. 22, no. 6, pp. 1488–1500, 2019.

[11] Y. Li, C. Li, Q. S. Li, Q. Song, X. Huang, and Y. G. Li, "Aerodynamic performance of CAARC standard tall building model by various corner chamfers," *Journal of Wind Engineering and Industrial Aerodynamics*, 2020.

[12] J. Xie, "Aerodynamic optimization of super-tall buildings and its effectiveness assessment," *Journal of Wind Engineering and Industrial Aerodynamics*, vol. 130, pp. 88–98, 2014.

[13] P. Irwin, J. Kilpatrick, J. Robinson, and A. Frisque, "Wind and tall buildings: negatives and positives," *The Structural Design of Tall and Special Buildings*, Wiley, Hoboken, NJ, USA, 2008.

[14] Y. G. Li, M. Y. Zhang, Y. Li, Q. S. Li, and S. J. Liu, "Experimental study on wind load characteristics of high-rise buildings with opening," *The Structural Design of Tall and Special Buildings*, Wiley, Hoboken, NJ, USA, 2020.

[15] P. W. Bearman, "The effect of base bleed on the flow behind a two-dimensional model with a blunt trailing edge," *Aeronautical Quarterly*, vol. 18, no. 3, pp. 207–224, 1967.

[16] H. Kikitsu and H. Okada, "Open passage design of tall buildings for reducing aerodynamics response," *Wind Engineering into the 21st Century*, CRC Press, Boca Raton, FL, USA, 1999.

[17] R. Dutton and N. Isyumov, "Reduction of tall building motion by aerodynamic treatments," *Journal of Wind Engineering and Industrial Aerodynamics*, vol. 36, no. 1–3, pp. 739–747, 1990.

[18] H. Okada and L. Kong, *The Effects of Open Passage on Reducing Wind Response of Tall Buildings*, Architectural Institute of Japan, Tokyo, Japan, 1997.

[19] Y. C. Zhang, Y. Qin, and C. G. Wang, "Research on the influence of openings to static wind load of high-rise buildings," *Journal of Building Structures*, vol. 25, no. 4, pp. 112–117, 2004, in Chinese.

[20] G. Hu, S. Hassanli, K. C. S. Kwok, and K. T. Tse, "Wind-induced responses of a tall building with a double-skin façade system," *Journal of Wind Engineering and Industrial Aerodynamics*, vol. 168, pp. 91–100, 2017.

[21] Q. S. Li, F. B. Chen, Y. G. Li, and Y. Y. Lee, "Implementing wind turbines in a tall building for power generation: a study of wind loads and wind speed amplifications," *Journal of Wind Engineering and Industrial Aerodynamics*, vol. 116, pp. 70–82, 2013.

[22] Q. S. Li, Z. R. Shu, and F. B. Chen, "Performance assessment of tall building-integrated wind turbines for power generation," *Applied Energy*, vol. 165, pp. 777–788, 2016.

[23] S. Hassanli, K. Chauhan, M. Zhao, and K. C. S. Kwok, "Application of through-building openings for wind energy harvesting in built environment," *Journal of Wind Engineering and Industrial Aerodynamics*, vol. 184, pp. 445–455, 2019.

[24] L. Wang, H. P. Wang, S. L. Wang, and J. Li, "Numerical study of wind pressure of high-rise building with openings," *Journal of Wuhan University of Technology*, vol. 34, no. 5, pp. 122–126, 2012.

[25] GB50009-2012, *Load Code for the Design of Building Structures*, China Architecture and Building Press, Beijing, China, 2012.

[26] Q. S. Li, F. B. Chen, S. H. Huang et al., "Feasibility investigations on wind power generation on top of super-tall buildings," *China Civil Engineering Journal*, vol. 45, no. 9, pp. 11–18, 2012, in Chinese.

[27] Y. C. Zhang, Y. Qin, and C. G. Wang, "Research on the influence of openings to static wind load of high rise buildings," *Journal of Building Structures*, vol. 25, no. 4, pp. 112–117, 2004, in Chinese.